CZECH TECHNICAL UNIVERSITY

IN PRAGUE

FACULTY OF MECHANICAL ENGINEERING

Modeling of flows with boundary layer transition

Jan Sedláček

Prague 2021

ZADÁNÍ DIPLOMOVÉ PRÁCE

I. OSOBNÍ A STUDIJNÍ ÚDAJE

Příjmení: **Sedláček** Jméno: **Jan** Osobní číslo: **459612**

Fakulta/ústav: **Fakulta strojní**

Zadávající katedra/ústav: **Ústav technické matematiky**

Studijní program: **Strojní inženýrství**

Studijní obor: **Matematické modelování v technice**

II. ÚDAJE K DIPLOMOVÉ PRÁCI

Název diplomové práce:

Modelování turbulentního proudění s přechodem v mezní vrstvě

Název diplomové práce anglicky:

Modeling of flows with boundary layer transition

Pokyny pro vypracování:

1) Podejte základní popis EARSM modelu turbulence a přechodového modelu gama-SST
2) Navrhněte propojení rovnice intermitence s EARSM modelem
3) Navržený model implementujte v prostředí OpenFOAM
4) Kalibrujte implementovaný model na vybraných případech obtékání desky
5) Model použijte pro řešení obtékání profilu či mříže. Výsledky srovnejte s experimentem.

Seznam doporučené literatury:

HELLSTEN, Antti K., 2005. New Advanced k-w Turbulence Model for High-Lift Aerodynamics. AIAA Journal [online]. 43(9), 1857–1869. ISSN 0001-1452. Dostupné z: doi:10.2514/1.13754
MENTER, Florian R., Pavel E. SMIRNOV, Tao LIU a Ravikanth AVANCHA, 2015. A one-equation local correlation-based transition model. Flow, Turbulence and Combustion [online]. B.m.: Flow, Turbulence and Combustion, 95(4), 583–619. ISSN 1386-6184. Dostupné z: doi:10.1007/s10494-015-9622-4
ROACHE, P. J., 1997. QUANTIFICATION OF UNCERTAINTY IN COMPUTATIONAL FLUID DYNAMICS. Annual Review of Fluid Mechanics [online]. 29(1), 123–160. ISSN 0066-4189. Dostupné z: doi:10.1146/annurev.fluid.29.1.123
MARIC, Tomislav, Jens HOPKEN a Kyle MOONEY, 2014. The OpenFOAM technology primer. ISBN 9783000467578.

Jméno a pracoviště vedoucí(ho) diplomové práce:

doc. Ing. Jiří Fürst, Ph.D., ústav technické matematiky FS

Jméno a pracoviště druhé(ho) vedoucí(ho) nebo konzultanta(ky) diplomové práce:

Datum zadání diplomové práce: **12.04.2021** Termín odevzdání diplomové práce: **15.08.2021**

Platnost zadání diplomové práce: _____

doc. Ing. Jiří Fürst, Ph.D. podpis vedoucí(ho) práce	doc. Ing. Jiří Fürst, Ph.D. podpis vedoucí(ho) ústavu/katedry	prof. Ing. Michael Valášek, DrSc. podpis děkana(ky)

III. PŘEVZETÍ ZADÁNÍ

Diplomant bere na vědomí, že je povinen vypracovat diplomovou práci samostatně, bez cizí pomoci, s výjimkou poskytnutých konzultací. Seznam použité literatury, jiných pramenů a jmen konzultantů je třeba uvést v diplomové práci.

. _____ Datum převzetí zadání

_____ Podpis studenta

Prohlášení

Prohlašuji, že jsem diplomovou práci s názvem: "Modelování turbulentního proudění s přechodem v mezní vrstvě" vypracoval samostatně pod vedením doc. Ing. Jiřího Fürsta, Ph.D. s použitím literatury uvedené na konci mé diplomové práce v seznamu použité literatury.

V Praze, June 4, 2021

Jan Sedláček

Poděkování

Tímto bych chtěl poděkovat panu doc. Ing. Jiřímu Fürstovi, Ph.D. za vedení, rady, odborné připomínky a ochotu při vypracovávání této práce. Také bych rád vyjádřil moje poděkování své rodině a přátelům, kteří mne podporovali po celou dobu studia.

Abstract

A three-equation model based around explicit algebraic Reynolds stress modelling is proposed. The model is built on an existing and tested model, namely, EARSM by Hellsten. As a third equation, it incorporates an intermittency equation to predict laminar-turbulent transitions in a boundary layer from $\gamma - SST$ by Menter. This new formulation aims to take the best from these two models, concretely the weak anisotropy and an ability to predict boundary layer transitions. The model was calibrated on a set of flat plate flows under various conditions, and its performance was tested on simple external and internal aerodynamics cases.

Keywords

Turbulence, k-Omega, gamma SST, OpenFOAM, CFD, fluid dynamics, Laminar-turbulent transition, Correlation, Local variables, explicit algebraic Reynolds stress model

Abstrakt

V této práci jsme se zabývali novou formulací trojrovnicového turbulentního modelu založeného na algebraickém Reynoldsově tensoru napětí. Model je vyvtořen na základech modelu EARSM navrženého Hellstenem a kol. [3]. Jako třetí, doplněná, rovnice je rovnice pro výpočet intermitence pomocí, které určujeme přechod z laminární to turbulentní mezní vrstvy. Formulace této rovnice je převzata z $\gamma - SST$ modelu navrženého Menterema kol. [4]. Tato nově navržená formulace modelu si dává za cíl převzít z existujících modelů jejich silné stránky. Konkrétně schopnost zachytit anisotropii proudění a schopnost spočítat přechodovou mezní vrstvu. Tento model byl kalibrován na souboru úloh obtékání rovné desky za různých okrajových podmínek. Výsledný model byl otestován na jednoduchých případech vnější a vnitřní aerodynamiky.

Klíčová slova

Turbulence, k-Omega, gamma SST, OpenFOAM, přechod v mezní vrstvě, korelace lokálních proměnných, explicitní algebraické Reynoldsovo napětí

Contents

List of Figures

List of Tables

List of used symbols and sings

II	second invariants of tensors $t_{ij}, a_{ij}, S_{ij}, \Omega_{ij}$, defined by their subscripts
III	third invariants of tensors $t_{ij}, a_{ij}, S_{ij}, \Omega_{ij}$, defined by their subscripts
IV	tensor invariant defined as $S_{kl}\Omega_{lm}\Omega_{mk}$
a_{ij}	Reynolds stress anisotropy tensor
$a_{ij}^{(ex)}$	explicit Reynolds stress anisotropy tensor
a_1	Bradshaw's structural parameter
β^*	EARSM model coefficient
$\beta_1, ..., \beta_9$	coefficients in the explicit tensor expression for the Reynolds stress anisotropy
c_p	heat capacity at constant pressure
c_l	lift coefficient
C_{TU}	critical Reynolds number coefficients
C_{PG}	F_{PG} function coefficients
CFD	Computational fluid dynamics
C, c	various constants in turbulence models defined by their subscripts
D_k	Destruction term from SST
δ_{ij}	Croneckers' delta
EARSM	Explicit algebraic Reynolds stress model
ϵ	turbulent dissipation rate
f_{mix}	mixing function for model coefficients
F	various constants in turbulence models defined by their subscripts
F_{length}	transition length function
F_{onset}	intermittency production trigger function
F_{lim}^{on}	production limiter function
F_3	blending function modification
F_{PG}	gradient switch function
$g - EARSM$	$\gamma - EARSM$
$g - SST$	$\gamma - SST$
$\gamma - Re_{theta}$	Langrty's transitional transport model
$\gamma - SST$	transitional transport model
γ	intermittency
γ_{earsm}	EARSM model constant
k/K	turbulent kinetic energy
$k - \omega SST$ / SST	Menter's shear-stress transport model
$k - \omega BSL$ / BSL	Menter's baseline $k - \omega$ model
L_t	characteristic length
LES	Large eddy simulation

$\lambda_{\theta L}$	local pressure gradient
λ_t	turbulent heat transfer coefficient
M_{1is}	isentropic inlet Mach number
μ	dynamic viscosity
μ_t	turbulent viscosity
ν	kinematic viscosity
ν_t	kinematic eddy viscosity
Ω_{ij}	mean vorticity tensor
Ω^*_{ij}	apparent net vorticity tensor
ω	specific turbulent dissipation rate
P_k^{lim}	additional production term
P_k	Production term from SST
Pr_t	turbulent Prandtl number
Pr	Prandtl number
Re_c	critical Reynolds number
Re_v	local vorticity Reynolds number
$Re_{\theta c}$	Critical momentum thickness Reynolds number
Re_x	Reynolds number, $\rho x U_{ref}/\mu$
R_T	viscosity ratio
RANS	*Reynolds averaged Navier-stokes*
ρ	fluid density
$\overline{\rho u_i' u_j'}$	Reynolds stress tensor
S_{ij}	mean strain-rate tensor
S_{ij}	mean strain-rate tensor
SST	*Shear stress transport*, přenos tečného napětí
σ	various constants in turbulence models defined by their subscripts
Tu_L	local turbulence intensity
T_{t1}	inlet total temperature
τ	scale variable in EARSM
τ_{ij}	laminar stress tensor
τ_{ij}^t	Reynolds stress tensor
τ^{CFD}	Total wall shear stress from numerical simulation
τ^{exp}	Total wall shear stress from experiment
u	velocity vector component u_i
x	Cartesian coordinate, x_i

1. Introduction

1.1 Thesis goal

This thesis aims to develop a new turbulence model, exploring the laminar-turbulent transition in the boundary layer. As CFD simulations become more mature over the last decades, the demand for more accurate results grew. In particular cases of CFD, the simplification to a fully turbulent boundary layer is not enough. This simplification becomes evident if we require more accurate knowledge of shear stress, separation point and other boundary layer phenomena dependent on the state of the boundary layer. Usually, the boundary layer contains laminar, transitional, and turbulent regions. We are looking for a branch of laminar-turbulent transitional turbulence models based on intermittency to model these phenomena. Specifically, such models are $\gamma - Re_\theta$ [2] model and its Galilean invariant modification $\gamma - SST$ [4]. The latter serves as a base for our turbulence model. We chose this model because it requires only a single additional equation to its base turbulence model $k-\omega$ SST [8], and thus we can reuse this equation for our model. The choice for our bedrock model landed on the EARSM model written by Hellsten [3]. As its name hints, this model is based on the algebraic Reynolds stress model formulation. This formulation significantly improves its performance over the $k-\omega$ BSL [8]. Furthermore, the algebraic tensor allows capturing the anisotropic properties of a flow. A combination of these models, as mentioned earlier, should provide us with a turbulence model which can capture the transition with higher accuracy than each of the models alone. We have modified and connected equations from the mentioned models to develop the turbulence model and later calibrated them to perform to our liking. Because of the way the model is created, we will refer to it in this thesis as $\gamma - EARSM$.

1.1.1 Transition turbulence models

At this point, we will step back for a short moment to quickly explain the circumstances of what we are modelling. The phenomena we are interested in is called turbulence, best described as a property of viscous fluid flow, which has attributes: non-deterministic flow fluctuations in both space and time; turbulent convection of mass, momentum and heat; vorticity, turbulent flow spatiality and dissipation of turbulent kinetic energy [24]. To see more on this topic, see [24]. We can start with a successful derivation and Reynolds averaging of Navier-Stokes equations. Generally, for an incompressible assumption, we use Reynolds averaging. With a compressible assumption, the combination with Favre averaging is more suitable. This set of simplifications and assumptions is referred to as RANS equations. After averaging, we are left with a new unknown term called Reynolds stress. This term has to be either resolved or modelled to close Navier-Stokes equations fully. Presently, the most widely used model for calculating the Reynolds stress term is the Boussinesq approximation, which replaces this term with a function of two new unknown

quantities. These unknown quantities are turbulence kinetic energy - k and some form of the rate of dissipation of turbulent kinetic energy. Most widely used turbulence models today thus contain two equations for the calculation of each unknown quantity. The most widely known models are some forms of $k-\epsilon$ [25], $k-\omega$ models [26]. ϵ being the rate of dissipation of turbulent kinetic energy, and ω is a specific rate of dissipation. However, there are other models which utilize different variables than these mentioned. As was already mentioned, we are interested in laminar-turbulent transition models. One drawback of the previously mentioned models is that they assume a fully turbulent flow and boundary layer. The latter restrain means that RANS and these equations generally cannot predict the transition, separation, etc. We can, however, lift this restriction if we try to model the transition between the laminar and turbulent boundary layer.

Transition is the phase in fluid flow, where the flow transitions from its laminar to a turbulent state. This transition is driven by several factors and widely differs between situations where the boundary layer transition occurs. Some of the elements are the interaction with the free-stream flow, surface roughness, Tollmien-Schlichting waves, initial conditions, separation, etc. However, to model all these phenomena is not yet plausible. Therefore, transitional turbulence models contain triggering functions with coefficients that are then empirically correlated with the experimental data. The most well-known transitional turbulent models are based on intermittency. The equation for the calculation of the intermittency contains the triggering functions. The most widely known model is probably called $\gamma - Re_\theta$ [2]. Another approach is 'physics-based model of the transition through laminar fluctuation energy [4].

1.2 Workflow

1.2.1 Implementation into OpenFOAM

We wrote the model to link all the appropriate terms and then was coded using the existing implementations of the models mentioned above, see further in section 2. The model is based on the EARSM model formulated by Hellsten, where the underlying formulation is a two-equation $k-\omega$ model. This model bears many similarities to the SST model up to one constant and the formulation of turbulence eddy viscosity. To stay true to his model, we have retained both f_{mix} and μ_t. Hellsten's formulation is then further interlinked with the intermittency equation through the production and destruction terms in the equation for ω.

1.2.2 Model calibration

For the calibration, we used the flat plate experiments [19],[23], as they are widely used for laminar-turbulent transitional turbulence model validation or calibration. These experiments observed and measured the properties of the fluid flow and the development of a boundary layer on a flat desk without a pressure gradient and an adverse pressure gradient, which simulates the suction side of the Rolls-Royce turbine blade. In our numerical studies, we created the pressure gradient by upper

surface curvature. The curvature parametric equation is in Chapter 3

To simulate the experiment, we have created a mesh in *BlockMesh*, which is the standard utility of the OpenFOAM package and an excellent tool for creating simple meshes of high quality. The next step was to define our computational domain simulating the ERCOFTAC wind tunnel setup. Furthermore, we used the base $\gamma - SST$ to fine-tune our boundary conditions to obtain numerical results that agree with the data from ERCOFTAC. Our boundary condition choices are in the table 3.2.

Then we had to calibrate the turbulence model coefficients on these test cases. Zero-pressure gradient test cases T3 were chosen as our base calibration upon which the adverse pressure gradient cases T3C were built. This workflow was chosen as zero-pressure cases contain the core physical phenomena, which all more complex cases accommodate. Since the model coefficients are highly interconnected, the calibration process was repeated several times to obtain the best combination. Optimization algorithms were integrated into our workflow to speed up the search for coefficients.

1.2.3 Complex validation simulations

In the final stage, we have chosen representative cases based on real-world application to validate our turbulence model and compared it with experimental values and other turbulence models, especially $\gamma - SST$ as we partially used this model. For that, we have chosen a two-dimensional simulation of an NLF-0416 airfoil at a wide range of angles of attack, then compared the resulting section characteristics and pressure distributions. Furthermore, we looked at the laminar to turbulent transition location. Another application case was the turbine blade cascade with a profile from Von-Karmán Institute for Fluid Dynamics [13]. Here we compared the skin-friction coefficient and velocities along the blade surface.

2. Theory

2.1 Model formulation

As was already foreshadowed in section 1, the mathematical model used during our calculations is called RANS, Reynolds Averaged Navier Stokes, which, as the name implies, is a form of the Navier-Stokes equations. However, before any model can be used, we have to connect the mathematical formulation with the physics of our problem through assumptions. In our case, we took up assumptions such as our fluid is viscous and fully turbulent. Moreover, depending on the particular case, we either assume a constant density or model our fluid with ideal properties through a constitutive equation. Since a turbulent flow is highly time-dependent and hard to model, averaging the quantities in the equations over a longer time results in turbulent equations less demanding to model. One way to do that is through a process called Reynolds averaging. Reynolds averaging is a statistical approach, where each quantity is divided into its average and time-dependent, fluctuating parts. This process is also called Reynolds decomposition. Each decomposed variable is then plugged back to the Navier-Stokes formulation, and the equations are time-averaged [24]. In the case of compressible fluid, Reynolds averaging produces unknown density fluctuation terms. To remove these terms, we combine the Reynolds averaging with Favre averaging. For further reading, see [24]. To show the basic formulation of RANS equations, we assume that the flow in each simulation will reach a steady-state and, therefore, no variable is time-dependent. However, the newly proposed turbulence model is possible to pair with time-dependent formulations of RANS equations as well. Below is the RANS formulation,

$$\begin{aligned}
&\frac{\partial}{\partial x_i}\left(\overline{\rho}\tilde{U}_i\right) = 0, \\
&\frac{\partial}{\partial x_j}\left(\overline{\rho}\tilde{U}_i\tilde{U}_j\right) = -\frac{\partial \overline{P}}{\partial x_i} + \frac{\partial}{\partial x_j}\overline{\tau}_{ij} - \overline{\rho u_i' u_j'}, \\
&\frac{\partial}{\partial x_j}\left(\overline{\rho}\tilde{h}\tilde{U}_j\right) = \tilde{U}_j\frac{\partial \overline{P}}{\partial x_j} + \overline{u_j'\frac{\partial P}{\partial x_j}} + \overline{\tau_{ij}\frac{\partial U_i}{\partial x_j}} - \frac{\partial \overline{q}_j}{\partial x_j} - \frac{\partial}{\partial x_j}\overline{\rho h' u_j'},
\end{aligned} \tag{2.1}$$

where the last equation is only used if we are assuming compressible fluid.

For us, the most important term in these equations is the term $-\overline{\rho u_i' u_j'}$, called Reynolds stress. This is an unknown quantity, which we are missing to have a fully closed system of partial differential equations. However, we cannot close RANS directly with the equations for Reynolds stress as they contain unknown correlations. However, we can approximate this Reynolds stress or approximate unknown quantities in the equations for the Reynolds stress [24]. In RANS equations, the most common way is the first approach using the Boussinesq hypothesis. This hypothesis assumes that the molecular transfer of momentum between shear layers in a fluid is analogous to turbulent momentum transfer [24]. To illustrate that, we can take Couette shear flow in a Newtonian fluid, where we state that the shear stress in the fluid is proportional to the shear rate, where the

proportionality is a scalar constant viscosity μ. In other words, we have a molecular transfer of momentum in the perpendicular direction to the flow. Due to the Brownian motion of molecules, there is an exchange of momentum between the fluid layers. If we assume that the turbulence is also random in motion, we can say that turbulent fluctuations are analogous to Brownian motion. Then we can use the same relation for shear stress such that the stress is proportional to the shear rate. In the case of two-dimensional incompressible boundary layer flow, the equation is

$$-\overline{\rho u_i' u_j'} = \tau_{ij}^t = \mu_t \frac{\partial \overline{u_i}}{\partial x_j} \tag{2.2}$$

Where the constant of proportionality is the turbulent viscosity μ_t. The Boussinesq hypothesis for a general compressible three-dimensional flow is

$$\tau_{ij}^t = 2\mu_t \left(S_{ij} - \frac{1}{3} \frac{\partial u_k}{\partial x_k} \delta_{ij} \right) - \frac{2}{3} \rho k \delta_{ij} \tag{2.3}$$

This, however, still does not close our system of equations, but only introduces new quantities to model. Concretely, the turbulence viscosity μ_t and turbulent kinetic energy k. At this point, various turbulence models come to light, specifically algebraic, single-equation and two-equation models. These models are formulated to calculate these unknown variables, namely, turbulence viscosity μ_t and turbulent kinetic energy k. Normally, these models contain equations, which are in the form of time-dependent convection-diffusion partial differential equations. They are written in a way that they either μ_t or both quantities are calculated with or through them [24]. For now, we will focus on the two-equation models, which are widely used across the industry. These almost always contain a single equation for turbulence kinetic energy. Whereas the turbulent viscosity is approximated by the relation in the form $\mu_t = \mu_t(k, \epsilon)$. The ϵ is called the dissipation of turbulent energy and can be written as

$$\epsilon = k^{3/2}/L_t, \tag{2.4}$$

where L_t is the characteristic length. Turbulence models thus are a way of closing our system of equations.

Last unknown term is in the enthalpy equation, concretely $\overline{\rho h' u_j'}$. Turbulent heat flux is modeled using additional turbulent thermal conductivity. This is equivalent to the momentum transfer assumption, which we used in the Bousinessq approximation. Therefore, we can write

$$-\overline{\rho h' u_j'} = \frac{\mu_t}{Pr_t} \frac{\partial \overline{h}}{\partial x_j} \tag{2.5}$$

$$Pr_t = \frac{\mu_t c_p}{\lambda_t} \tag{2.6}$$

Last term is the

$$\frac{\partial \overline{q_j}}{\partial x_j} \tag{2.7}$$

which can be approximated as laminar thermal heat flux, which is formulated as follows

$$\frac{\partial \overline{q_j}}{\partial x_j} = \frac{\mu}{Pr} \frac{\partial \overline{h}}{\partial x_j} \tag{2.8}$$

These assumptions introduced several new variables, Pr_t, μ, Pr. However, these variables as usually assumed constant. In case Pr_t its value is usually in range $\langle 0.85, 0.9 \rangle$ [24].

2.1.1 $\gamma - \mathbf{SST}$ model

From Menter's formulation $\gamma - SST$ is written as

$$\begin{aligned}
\frac{\partial}{\partial t}(\rho k) + \frac{\partial}{\partial x_j}(\rho u_j k) &= \tilde{P}_k + P_k^{\lim} - \tilde{D}_k + \frac{\partial}{\partial x_j}\left[(\mu + \sigma_k \mu_t)\frac{\partial k}{\partial x_j}\right] \\
\frac{\partial}{\partial t}(\rho \omega) + \frac{\partial}{\partial x_j}(\rho u_j \omega) &= \alpha \frac{P_k}{v_t} - D_\omega + C d_\omega + \frac{\partial}{\partial x_j}\left[(\mu + \sigma_\omega \mu_t)\frac{\partial k}{\partial x_j}\right] \\
\frac{\partial(\rho\gamma)}{\partial t} + \frac{\partial(\rho u_j \gamma)}{\partial x_j} &= P_\gamma - E_\gamma + \frac{\partial}{\partial x_j}\left[\left(\mu + \frac{\mu_t}{\sigma_\gamma}\right)\frac{\partial \gamma}{\partial x_j}\right]
\end{aligned} \tag{2.9}$$

The Intermittency variable is a percentage representation of the time at which the boundary layer turbulent fluctuations are present. In laminar flow, that equals to zero and in fully turbulent, that equals to one [16][2]. where chosen, functions from the k and ω equations are written below,

$$\begin{aligned}
\tilde{P}_k &= \gamma P_k \\
P_k &= \mu_t S \Omega \\
\tilde{D}_k &= \max(\gamma, 0.1) \cdot D_k \\
P_k^{lim} &= 5 C_k \max(\gamma - 0.2, 0)(1-\gamma) F_{on}^{lim} \max(3 C_{SEP}\mu - \mu_t, 0) S\Omega
\end{aligned} \tag{2.10}$$

Term P_k^{lim} is added to support the production of k and in regions with low turbulence levels. $k - \omega SST$ as stated by Langtry has problems with the production of turbulence intensity and requires a relatively long-running length [2]. Selected terms from γ equation are

$$\begin{aligned}
P_\gamma &= F_{length} \rho S \gamma (1-\gamma) F_{onset} \\
E_\gamma &= c_{a2} \rho \Omega \gamma F_{turb}(c_{e2}\gamma - 1)
\end{aligned} \tag{2.11}$$

and the turbulent viscosity is written as

$$\mu_t = \rho \frac{a_1 \cdot k}{\max(a_1 \cdot \omega, F_2 \cdot S)} \tag{2.12}$$

Another critical variable is F_{length}, representing the transition length of the boundary layer. F_{onset} is then responsible for production initiation, and it is the function in which we are most interested [4].

2.1.2 EARSM model

Since the assumptions tied to the Boussinesq closure are pretty limiting and in a broad range of applications, the assumptions do not perform well. To mitigate some of these limitations, we have chosen an explicit algebraic stress turbulence model. These models are based on the observation that the ratio between the turbulent shear stress and the turbulent kinetic energy does not change much in thin shear layers. And thus allow the formulation of Reynolds stress with Reynolds-stress anisotropy tensor a_{ij} as follows [3][24],

$$a_{ij} = \frac{\overline{\rho u_i' u_j'}}{\overline{\rho} k} - \frac{2}{3}\delta_{ij} \tag{2.13}$$

"In flows where the anisotropy varies slowly in time and space, the transport equation for the Reynolds stress anisotropy tensor is reduced to an implicit algebraic relation"[17]. However, the

implicit formulation has many drawbacks. An explicit formulation was proposed by [18] to solve some of the problems of the implicit formulation. Advantage of such formulation is a faster computation time than in the case of six equations for Reynolds stresses. The integration is done by expansion of the Bousinessq approximation with the algebraic stress tensor, as visible below

$$\tau_{ij}^{t} = 2\mu_t \left(S_{ij} - \frac{1}{3}\frac{\partial u_k}{\partial x_k}\delta_{ij} \right) - \frac{2}{3}\rho k \delta_{ij} - a_{ij}^{(ex)} \rho k \tag{2.14}$$

With the algebraic stress tensor in an explicit form

$$\begin{aligned} a_{ij}^{(ex)} &= \beta_3 \left(\Omega_{ik}^{*}\Omega_{kj}^{*} - \frac{1}{3} II_{\Omega}\delta_{ij} \right) + \beta_4 \left(S_{ik}\Omega_{kj}^{*} - \Omega_{ik}^{*}S_{kj} \right) \\ &+ \beta_6 \left(S_{ik}\Omega_{kl}^{*}\Omega_{lj}^{*} + \Omega_{ik}^{*}\Omega_{kl}^{*}S_{lj} - II_{\Omega}S_{ij} - \frac{2}{3} IV \delta_{ij} \right) \\ &+ \beta_9 \left(\Omega_{ik}^{*}S_{kl}\Omega_{lm}^{*}\Omega_{mj}^{*} - \Omega_{ik}^{*}\Omega_{kl}^{*}S_{lm}\Omega_{mj}^{*} \right) \end{aligned} \tag{2.15}$$

The standard formulation of EARSM turbulence model as developed by Hellsten [3] is written as

$$\begin{aligned} \frac{\mathrm{D}(\rho k)}{\mathrm{D}t} &= P - \beta^{*} k\omega + \frac{\partial}{\partial x_j}\left[(\nu + \sigma_k \nu_T) \frac{\partial k}{\partial x_j} \right], \\ \frac{\mathrm{D}(\rho \omega)}{\mathrm{D}t} &= \gamma_{earsm} \frac{\omega}{k} P - \beta \omega^2 + \frac{\partial}{\partial x_j}\left[(\nu + \sigma_\omega \nu_T) \frac{\partial \omega}{\partial x_j} \right] + \frac{\sigma_d}{\omega} \max\left(\frac{\partial k}{\partial x_j}\frac{\partial \omega}{\partial x_j}; 0 \right) \end{aligned} \tag{2.16}$$

Since the model contains quantity γ, which in the case of EARSM is constant, it represents intermittency in $\gamma - SST$. For the sake of clarity, in this paper, we will retype γ from EARSM to γ_{earsm}. Main functions and quantities printed below, for further reading, see [3].

$$\begin{aligned} P &= \tau_{ij}\frac{\partial u_i}{\partial x_j} \\ S_{ij}^{*} &= \frac{\tau}{2}\left(\frac{\partial u_i}{\partial x_j} + \frac{\partial u_j}{\partial x_i} \right) \qquad \Omega_{ij}^{*} = \frac{\tau}{2}\left(\frac{\partial u_i}{\partial x_j} - \frac{\partial u_j}{\partial x_i} \right) - \frac{\tau}{A_0}\Omega_{ij}^{(r)} \\ \tau &= \max\left(\frac{1}{\beta^{*}\omega}, 6.0\sqrt{\frac{\nu}{\beta^{*} k\omega}} \right) \end{aligned} \tag{2.17}$$

with turbulent viscosity written in form

$$\mu_t = C_\mu k \tau \qquad C_\mu = -\frac{1}{2}\left(\beta_1 + \mathrm{II}_{\Omega}\beta_6 \right) \tag{2.18}$$

2.1.3 Proposed formulation of a new model γ – EARSM

As we said in the chapter1 we took EARSM model as our starting point. Then we took over Menter's formulation of the intermittency equation without modification, however to interconnect these models, we had to modify the EARSM formulation as follows,

$$\begin{aligned} \frac{\mathrm{D}(\rho k)}{\mathrm{D}t} &= \gamma \mu_t S\Omega + P_k^{lim} - max(\gamma, 0.1) * \beta^{*} k\omega + \frac{\partial}{\partial x_j}\left[(\nu + \sigma_k \nu_T) \frac{\partial k}{\partial x_j} \right], \\ \frac{\mathrm{D}(\rho \omega)}{\mathrm{D}t} &= \gamma_{earsm} \frac{\omega}{k} P - \beta \omega^2 + \frac{\partial}{\partial x_j}\left[(\nu + \sigma_\omega \nu_T) \frac{\partial \omega}{\partial x_j} \right] + \frac{\sigma_d}{\omega} \max\left(\frac{\partial k}{\partial x_j}\frac{\partial \omega}{\partial x_j}; 0 \right), \\ \frac{\mathrm{D}(\rho \gamma)}{\mathrm{D}t} &= P_\gamma - E_\gamma + \frac{\partial}{\partial x_j}\left[\left(\mu + \frac{\mu_t}{\sigma_\gamma} \right) \frac{\partial \gamma}{\partial x_j} \right] \end{aligned} \tag{2.19}$$

To connect the intermittency equation with the existing EARSM model, we had to modify the production destruction terms and add a production limiter to incorporate intermittency γ terms.

Furthermore, we have left the turbulence viscosity μ_t untouched to not interfere with the Hellsten's implementation.

The production and destruction terms are as follows:

$$\begin{aligned} P &= \tau_{ij}\frac{\partial u_i}{\partial x_j} \\ P_\gamma &= F_{length}\rho S\gamma(1-\gamma)F_{onset} \\ E_\gamma &= c_{a2}\rho\Omega\gamma F_{turb}(c_{e2}\gamma - 1) \\ P_k^{lim} &= 5C_k \max(\gamma - 0.2, 0)(1-\gamma)F_{on}^{lim}\max(3C_{SEP}\mu - \mu_t, 0)S\Omega \end{aligned} \tag{2.20}$$

Specifically, the transition onset F_{onset} is calculated through a series of expressions,

$$\begin{aligned} F_{onset} &= \max(F_{onset2} - F_{onset1}, 0), \qquad F_{onset1} = \frac{Re_v}{2.2Re_{\Theta c}} \\ F_{onset2} &= \min(F_{onset1}, 2.0), \qquad F_{onset3} = \max\left(1 - \left(\frac{R_T}{3.5}\right)^3, 0\right) \end{aligned} \tag{2.21}$$

$$F_{turb} = e^{-\left(\frac{R_T}{2}\right)^4}, \quad R_T = \frac{\rho k}{\mu\omega}, \quad Re_v = \frac{\rho d_w^2 S}{\mu} \tag{2.22}$$

To trigger the production of γ we have to calculate Re_c, which sets the critical Reynolds number, where the transition should occur. It is a function of local variables, concretely Local turbulence intensity Tu_L and local pressure gradient $\lambda_{\Theta L}$. The formulation of the critical Reynolds number is

$$Re_{\Theta c} = C_{TU1} + C_{TU2}e^{-C_{TU3}Tu_L F_{PG}} \tag{2.23}$$

Local turbulence intensity is responsible for the turbulence intensity levels inside the boundary layer, similar to free-stream values. $\lambda_{\Theta L}$, on the other hand, functions more like a shape function since it is not based on the pressure field but rather on the velocity field [4].

$$Tu_L = \min\left(100\frac{\sqrt{\frac{2k}{3}}}{\omega d_\omega}, 100\right), \qquad \lambda_{\Theta L} = \min\left(\max\left(-7.57\cdot 10^{-3}\frac{dV}{dy}\frac{d_\omega^2}{\nu} + 0.0128, -1.0\right), 1.0\right) \tag{2.24}$$

where the min-max formulation of $\lambda_{\Theta L}$ is for numerical robustness, see further [2]. The last variable of interest is the F_{PG} function. As Menter [4] have written "The function $F_{PG}(\lambda_{\Theta L})$ is introduced to sensitize the transition onset to the streamwise pressure gradient." Concretely, when we are calculating the model without pressure gradient, $Re_{\Theta c}$ is constant as the local turbulence intensity is zero. The function reads as:

$$F_{PG} = \begin{cases} if(\lambda_{\Theta L} \geq 0) & \max(\min(1 + C_{PG1}\lambda_{\Theta L}, C_{PG1}^{lim}), 0.0) \\ if(\lambda_{\Theta L} < 0) & \max(\min(1 + C_{PG2}\lambda_{\Theta L} + C_{PG3}\min(\lambda_{\Theta L} + 0.0681, 0), C_{PG2}^{lim}), 0.0) \end{cases} \tag{2.25}$$

As will be shown in chapter 4, when calculated numerically, the local pressure gradient, which is a function of velocity, can trigger F_{PG} even in zero pressure gradient conditions.

3. Model development

3.1 Model calibration

For the basic calibration of the turbulence model, a set of ERCOFTAC flat-plate experiments was used. This experimental data consists of zero pressure gradient T3A, T3B, and T3A- cases and cases with adverse pressure gradients T3C2, T3C3, T3C4 and T3C5.

3.1.1 Calibration workflow

At the beginning of our coefficient calibration, we created three domains, which differ in geometry. The first domain type is a rectangular channel of constant height made for all zero pressure gradient cases. Together they are referred to as T3 cases. The second type of domain is for the T3C4 case, with an upper wall profile based on equation (3.2), where the slip boundary condition is applied. The last type is for the rest of the adverse pressure gradient cases, T3C2, T3C3, and T3C5. The upper wall has a curvature defined by equation (3.3). The numerical boundary conditions are the same across all named cases. The commonality, however, ends here as each case requires unique boundary condition values.

We do not need to calibrate all constants again for the calibration itself, only those responsible for the boundary layer transition. Since we are building our new turbulence model out of two already existing and calibrated models, our main goal is to model the boundary layer transition correctly. We will focus on adjusting the intermittency equation coefficients such that our turbulence model sufficiently approximates all experimental test cases T3 and T3C. Calibration of only the intermittency equation will ease the workload, as we do not need to calibrate the whole model again. Specifically, our focus is on matching the total wall shear stress with the experimental data. We calculated the total wall shear stress as the surface area under the skin friction coefficient curves for experimental and numerical data. Specifically, we minimised the error function reads

$$err = \sqrt{\left(\int_{x_1}^{x_2} \tau^{CFD} - \tau^{Exp} dx \right)^2}, \tag{3.1}$$

where our x_1 and x_2 were our first, respectively, last experimental data points. Another good approach would be to align the $Re_{\Theta c}$ with the experiment or the midpoint of the transition line. Midpoint matching can be done, for instance, by finding the maximum gradient of c_f in the transition section. The latter approach would approximate the point of transition.

3.1.2 ERCOFTAC calibration

ERCOFTAC wind tunnel experiment encapsulates the test surface, an inverted flat plate with a leading edge of radius 75 mm and 1.7 m in total length and boundary layer bleed and pressure

gradient diffusing wall. The measurement probes are only in a length of 1.5 m. For detail see [22], [23] and figure 3.1. The experiment setup is able to provide a pressure gradient to mimic

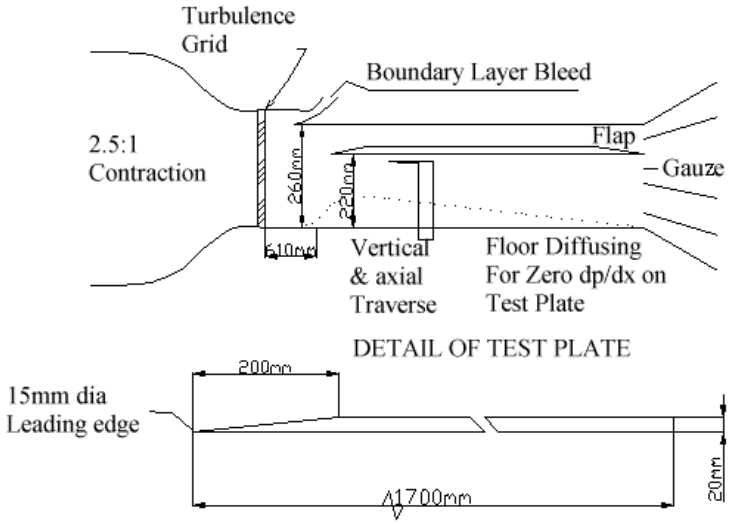

Figure 3.1: Setup of flat plane wind tunnel experiment see[23]

the pressure distribution on the turbine blade suction side. In our case, the pressure gradient is provided by shaping the mesh's upper surface of the domain to simulate the suction side of the turbine blade. For the shape, the polynomial equation from [9] was used as follows

$$y(x) = 1.231x^6 - 6.705x^5 + 14.061x^4 - 14.113x^3 + 7.109x^2 - 1.900x + 0.950 \tag{3.2}$$

where equation (3.1) corresponds to the upper surface of cases T3C2,T3C3, and T3C5.

$$y(x) = 1.356x^6 - 7.591x^5 + 16.513x^4 - 17.510x^3 + 9.486x^2 - 2.657x + 0.991 \tag{3.3}$$

Eq. (3.2) approximates the upper surface of T3C4.

We run the simulation as a two-dimensional with *simpleFoam* solver. Our selection of two dimensions significantly simplifies the case, especially concerning computational time. Furthermore, we acknowledge that turbulent flow and phenomena concerning the boundary layer are spatial in nature. However, their effect in our case is negligible. *simpleFoam* is a solver for incompressible fluid in steady-state. It is based on the finite volume method and the computational algorithm named SIMPLE. It is an algorithm where we solve the equation for pressure and velocity separately. We have chosen 2^{nd} order numerical scheme with cell-limited gradient. Since the flow we are observing is deeply below the widely accepted value of $Ma \approx 0.3$ above which we should account for compressibility, its usage is adequate in these cases.

All mentioned validation and application cases were run with constant air properties defined through $\nu = 1.5 \cdot 10^{-5}[m^2/s]$ if not stated otherwise.

Geometry and boundary conditions

The geometry is in the shape of a cuboid, spanning from $x =< -0.05; 1.6 > [m]$. The left side has a boundary condition of velocity inlet. The right side has a pressure outlet. On the upper side, we

have a slip condition. On the bottom 0.05 m from the left side, we have a slip wall, from $x = 0.0$ till the right side, there is a no-slip condition. The mesh was in adherence with the information in Appendix of Menter; Smirnov; Liu; Avancha[4]. Concretely, the issue around y^+, where lowering y^+ further below 1, can move the laminar-turbulent transition curve further away from the transition curve obtained from the experiment. We observed this behaviour within our mesh also. We heightened the region for the T3C cases since the original height had a more unsatisfactory

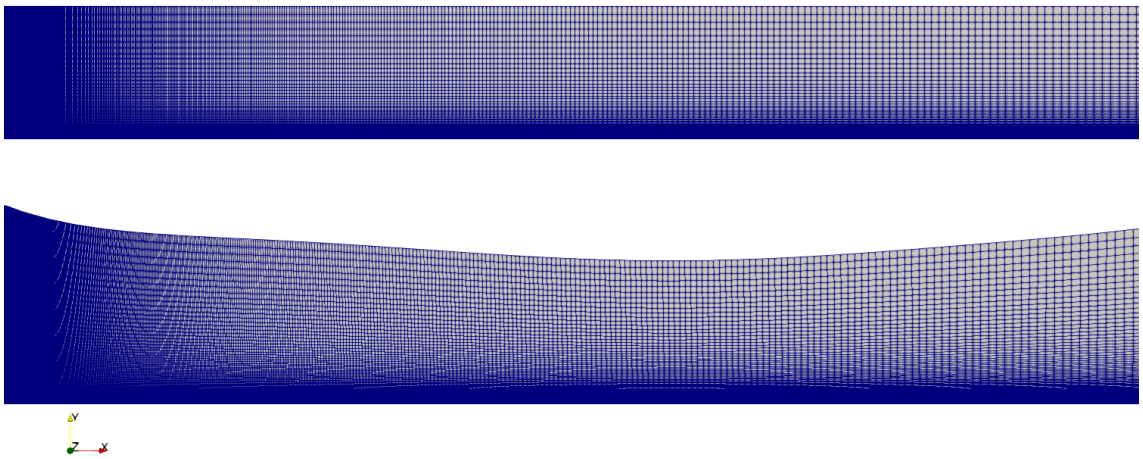

Figure 3.2: Representative visualization of meshes. Upper one is for zero pressure gradient cases, meanwhile lower mesh is for adverse pressure cases.

performance. The upper boundary wall curvature distorts the mesh in the region where the transition occurs. Figure 3.2 meshes are visible representative for zero and adverse pressure gradient. We do not present the mesh for the T3C4 case as it is visually almost identical to the adverse pressure gradient mesh at this scale. These sizes provide the best trade-off between computational time, quality of results, and the mesh. Another factor was steer clear from having a large skewness ratio and extreme values of minimal and maximal y^+. The main simplification introduced into our mesh was removing the front edge radius and substituting it with a sharp edge. Missing edge is acknowledged during the model calibration as it could slightly offset the initial rundown of the friction coefficient around the start of the flat plane. However, the transition point position and slope should not be affected.

On the figure below are shown results from the grid convergence study using Roaches Grid Convergence Index (GCI) [14]. For this study, we have created three meshes with two times increase in the total number of grid points above the plate, see Table 3.1. All tested meshes used the same total expansion ratio of 80 in x-direction and 500 in the y-direction. As a representative variable to describe the grid convergence, we used the ratio of Re_x between the experiment and numerical results. From the experiment, we took the data point located in the middle of the transition $[2.38 \cdot 10^5, 0.00375]$ and its corresponding value of Re_x. From the numerical simulation of the T3A

Grid	Number of vertices	Re_x ratio	no. of cells (x,y)
1	15750	0.8840	(315,50)
2	31500	0.9474	(500,65)
3	63000	0.9654	(600,105)

Table 3.1: Grid information and difference between numerical and experimental transition midpoint

case, we took Re_x for the same value of $c_f = 0.00375$.

$$Re_x \text{ ratio} = \left(\frac{Re_x^{num}}{Re_x^{exp}} \right)_{c_f=0.00375} \tag{3.4}$$

For GCI, we have used $\gamma - SST$ as our turbulence model. After checking if the solutions are in the asymptotic range of convergence

$$\frac{3.236058}{2^{1.845737}0.883800} = 1.018686 \tag{3.5}$$

which is approximately equal to one, we can conclude that we are within the asymptotic range. To visualize the transition curves, see figure 3.4. It is visible that the difference between the two

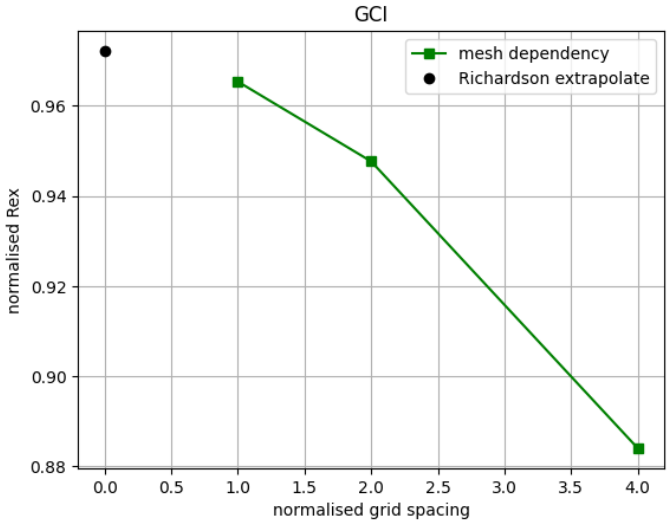

Figure 3.3: grid convergence study using GCI

finer meshes is small. Based on this study, we can conclude that the mesh number three from table 3.1 does not affect the results obtained with this mesh. The mesh size for adverse pressure gradient cases was chosen separately mesh size of *125x600* cells to mitigate the increased height of the domain.

Boundary conditions

Since we have created our mesh, the boundary conditions must be tested and adjusted for the numerical results to fit the experiment. For this initial setup of boundaries, we used the original $\gamma - SST$ turbulence model. Furthermore, as a base case, we used the values measured during the

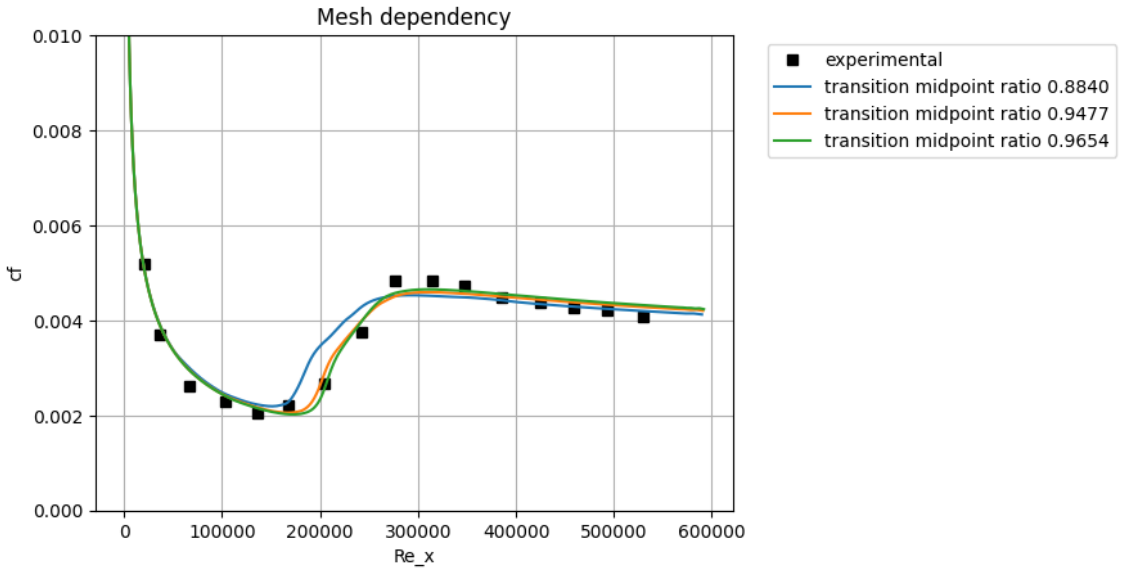

Figure 3.4: Visualization of transition curves from GCS

ERCOFTAC experiment. Since the data does not contain specific turbulence dissipation ω, it was calculated using these relations

$$\omega = \frac{k}{\eta}\left(\frac{\mu_t}{\mu}\right)^{-1} \tag{3.6}$$

$$k = \frac{3}{2}(UI)^2 \tag{3.7}$$

Data from the wind tunnel are measured at the beginning of the flat plane. However, we are imposing our condition 0.05m further away from the leading edge. Therefore, a slight adjustment was required to fit Tu to the experimental values. In the table below, we can see the optimised boundary conditions for the calibration of our model. Boundary condition readiness was judged

Case	ERCOFTAC data		Menter's $\gamma - SST$			Used		
	U0[m/s]	Tu [%]	U0[m/s]	Tu [%]	$\mu_t/\mu(\omega)$	U0[m/s]	Tu [%]	ω
T3A	5.4	3.0	5.18	3.3	12 (243)	5.4	3.3	264
T3A-	19.8	0.9	19.8	0.9	8.0 (397)	19.8	0.9	397
T3B	9.4	6.0	9.4	6.2	90 (377)	9.4	6.2	353
T3C2	5.0	3.0	5.29	3.0	8.0 (314)	5.29	3.0	320
T3C3	3.7	3.0	4.0	3.0	5.0 (288)	4.0	3.0	288
T3C4	1.2	3.0	1.37	3.0	2.0(84)	1.2	3.0	21
T3C5	8.4	3.0	9.0	3.0	15.0(486)	9.0	3.0	360

Table 3.2: reference boundary conditions

through a pair of graphs of $C_f - Re_\Theta$ and $Tu - Re_\Theta$, where the best fit to the experimental data was taken.

Coefficient calibration

Our focus was on the coefficients in the γ production terms as we need to match the transition correctly. On the first run, without doing any modification, the transition curve has a visible aft shift of the experimental transition curve. Since Menter's turbulence model was designed, so that the coefficients $F_{length}, C_{TU1}, C_{TU2}, C_{TU3}$ are model parameters and as such are meant to be adjusted by the user. Our main goal is to match the experimental results using only these parameters. As Langtry defined 'F_{length} in Eq. (3.4) is an empirical correlation that controls the length of the transition region'[2]. Therefore we will use F_{length} as our first coefficient. Furthermore, Langtry showed the effect of this parameter, where for higher values of F_{length}, the transition is smoother. On the other hand, lower values produce a sharper transition. Concretely, the values used by Langtry are 1, 28 & 100. Thus, we tried these values for our calibration as is visible in graph 3.5. Contrary to Langtry, our transition curve does not smoothen with decreasing F_{length}.

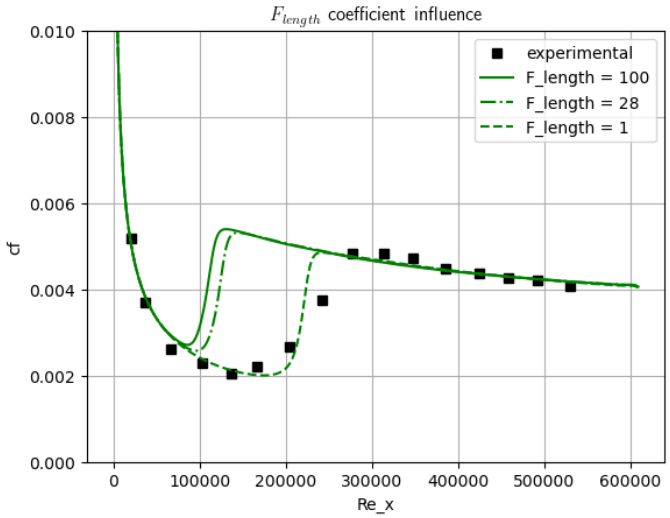

Figure 3.5: Influence of F_{length} on the case T3A

From graph 3.6 we can conclude that increasing C_{TU1} does move the transition downstream. There is also a slight difference in how does the curve behave in the turbulent boundary layer region.

If we look at the effect of C_{TU2} we can see that the coefficient has a much smaller influence on the transition position, even though the change in the coefficient value is also $\pm 50\%$, see 3.7.

The coefficient C_{TU3} differs in that with increasing value the transition moves upstream compared to other C_{TU}. Furthermore, it does not move evenly. Changing the value to 0.5 makes the curve almost match the transition position in the experiment. At least in the case of T3A, C_{TU3} influence is more comparable to the of F_{length} than other C_{TU}.

We have just shown the influence of each of the four coefficients on the transition curve. Since we have no way of knowing which combination will bring the experiment-like results, we use a minimisation algorithm to find the best combination of the coefficients. To add, we have observed their effect on the case T3A, but there is no way of knowing if the effect will be the same across all

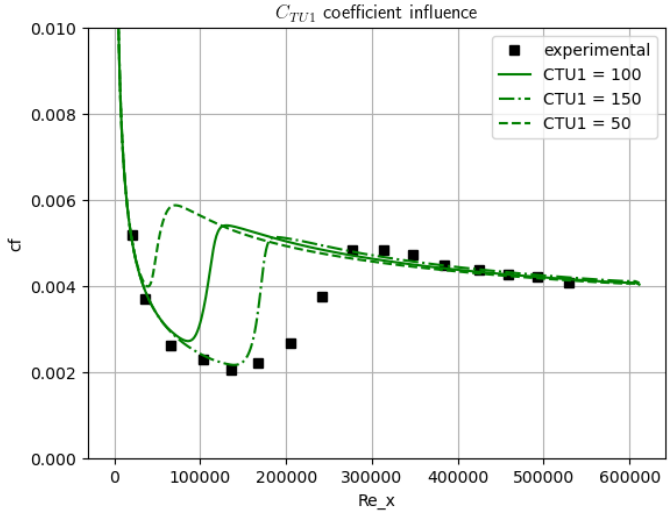

Figure 3.6: Influence of C_{CTU1} on the case T3A

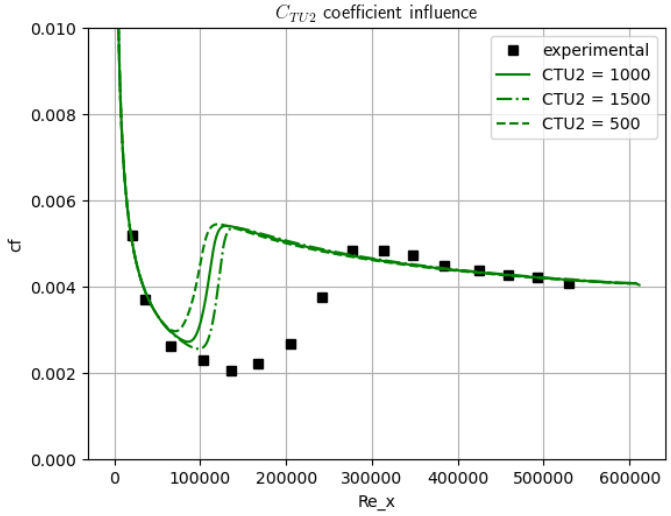

Figure 3.7: Influence of C_{CTU2} on the case T3A

other validation cases, and we know that it is not. To set at least some boundaries, we will adhere to Langtry [2] and use the aforementioned F_{length} values, explicitly 1, 28, and 100. Therefore, we will have three different sets of coefficients, among which we will choose based on their performance in our validation cases.

As a minimised variable, we have chosen the L2 norm of the differences between areas under the numerical and experimental result's skin friction curve. The curve is taken from the $c_f - Re_\Theta$ graph of each simulation. To obtain the area, we have numerically integrated the skin friction curve using the Simpsons rule. For the optimisation algorithm, our choice fell on Constrained Optimisation By Linear Approximation (*COBYLA*). COBYLA is a gradient-free minimisation algorithm using a linear approximation to the objective function. We implemented the algorithm in python script from *SciPy*, which is python's package based around the open-source software of the same name, see [20]. The disadvantage of *COBYLA* (and of most minimisation algorithms)

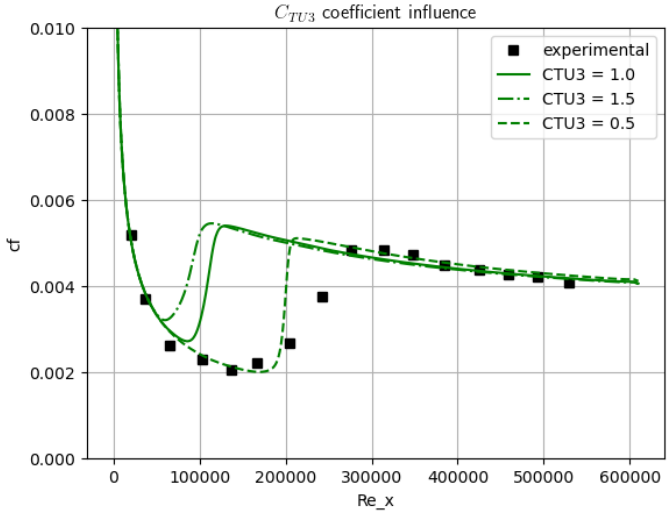

Figure 3.8: Influence of C_{CTU3} on the case T3A

is that they cannot guarantee to find global minima. However, to help the algorithm operating correctly, each coefficient was scaled to range $\langle 0, 1 \rangle$, where the original values corresponding to the scaled value of 0.5 in each coefficient. *COBYLA* can then take steps of the same size in each variable. Before writing in *turbulenceProperties* file, the values were scaled appropriately back.

Zero pressure gradient

The optimisation is built from physically simpler cases towards the complex ones, as the physical phenomena only add up. The simplest cases in our validation battery are zero pressure gradient cases T3. During the optimisation, we have introduced some constraints on the *COBYLA* algorithm. Concretely C_{TU1} was given bounds $\langle 0.1, 0.75 \rangle$, C_{TU2} & C_{TU3} were bounded between $\langle 0.1, 1.0 \rangle$. This bounding was based on our previous study of coefficient sensitivity. Furthermore, we set the bound violation step to 0.025 for all coefficients. However, the optimisation algorithm did not utilise the boundary violation constrain. Initial step was set to 0.25 with initial condition $C_{TU1} = 0.2, \quad C_{TU2} = 0.75, \quad C_{TU3} = 0.75$. In T3A, the difference between the c_f values for laminar and turbulent boundary layer is vast using CFD. Therefore we can never truly match the experimental results, and *COBYLA* algorithm would prefer for the transition never to occur, which is not ideal as the transition visibly occurs near the end of the plate, just not as severely as our model predicts. To counter this, we have increased the area below the experimental curve by 20%. In the table 3.3 are calculated the final coefficients, As we can see, *COBYLA* has fitted all cases well, where best performance can be with $F_{length} = 28$ and worst in case of $F_{length} = 1$. The last-mentioned produced the transition in T3A later than the other two coefficients sets. In the case of T3A- the performance is similar among all three variations and fits our expectations. We can further see that in case T3B the best performance had a set of coefficients with $F_{length} = 100$. Turbulence intensity values remained independent of the coefficients.

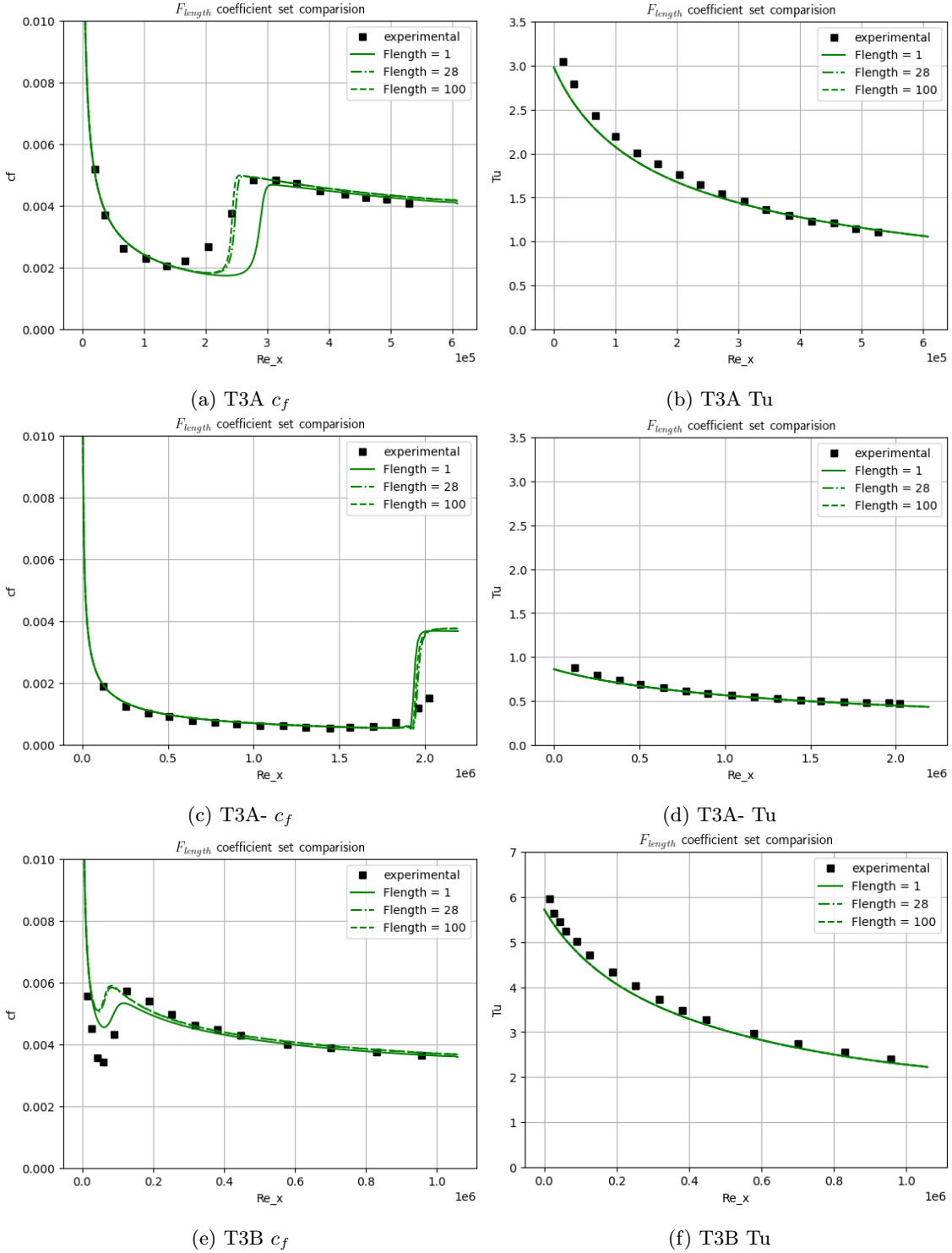

(a) T3A c_f

(b) T3A Tu

(c) T3A- c_f

(d) T3A- Tu

(e) T3B c_f

(f) T3B Tu

Figure 3.9: Results from coefficient calibration on zero pressure gradient cases showed on transition curve

Non-zero pressure gradient

When looking at the results obtained on T3C cases, we can, in general, see a pretty good fit. If we consider the T3C2, all three versions suffer from separation at $Re_x = 0.6 \cdot 10^6$, which does not occur in the experiment. However, the skin friction curve recovers to match the experimental

Coefficient values			
F_{length}	C_{TU1}	C_{TU2}	C_{TU3}
1	156	1420	1.08
28	172	1480	0.64
100	158	1380	0.54

Table 3.3: Coefficient values from optimization

values towards the end of the flat plate. This problem is present in the T3C3 case as well. The worst performance is visible in T3C4, where the curve does not recover from the separation. T3C5 is the best performing case among these. This case is in terms of boundary conditions and $Re_{\Theta c}$ closest to T3A, and therefore we expected a good C_f fit. Overall, the behaviour of $\gamma - EARSM$ does not deviate much from the $\gamma - SST$ performance in these validation cases. The reason for the otherwise poor performance is the fact that we have not used adverse pressure gradient cases for the calibration itself, rather just as a confirmation that with well-calibrated F_{length} and C_{TU} we can fit T3C cases as well.

As we cannot neglect the performance in the T3C case, a second optimisation is needed. As our base coefficient, we selected $F_{length} = 28$ because of its performance in T3. For the second optimisation, our optimisation algorithm of choice was SHGO. As a COBYLA, it is also a constrained, derivative-free optimisation algorithm. However, SHGO is a global optimisation algorithm. COBYLA works best when a function has a single local minimum. Although it cannot be proven, the single local minimum condition is plausible in the previous C_{TU} coefficients optimisation. However, when we incorporate another four coefficients, the plausibility seems less likely, and our optimisation would be dependent on a correct guess of the initial vector $\vec{x_0}$. For that reason, we have chosen SHGO, which is a global optimisation algorithm with ensured convergence to a global minimum. Still, in our case and with the hardware at hand, finding the global minimum is not plausible from the time perspective. To calculate our error function for a single optimisation step, we require all cases to be calculated, which is quite time-consuming. The optimisation was, therefore, ended after reaching sufficient values.

Range of optimized coefficients were extended by C_{PG1}, C_{PG2}, C_{PG2}^{lim} and C_{PG3}. Even though the regions of poor performance are in the area of adverse pressure gradient, we have included C_{PG1} to optimise the F_{PG} function as a whole. C_{PG2}^{lim} was taken into account because we have found from the observation that to see improvements in laminar to turbulent transition from C_{PG2} we have to alter the upper limit as well. C_{PG3} in the case of $\gamma - SST$ was set to 0, however Menter; Smirnov; Liu; Avancha states that "C_{PG3} becomes active in regions with separation, allowing correcting the $Re_{\Theta c}$ value there if necessary."In theory, this coefficient could help us recover in the regions with separation. Bounding for C_{TU} stayed the same as in the first minimisation. Values for C_{PG} coefficients were bounded by a maximum of ten times their initial value. We ran optimisation for all cases and therefore included both zero and adverse pressure gradients. Results are visible in

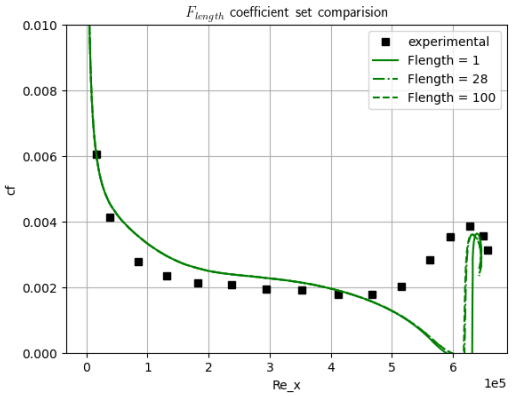

(a) T3C2 c_f

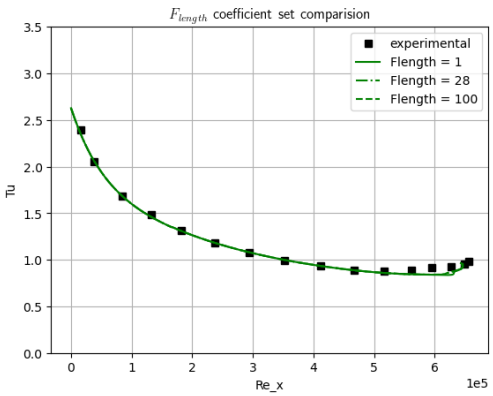

(b) T3C2 Tu

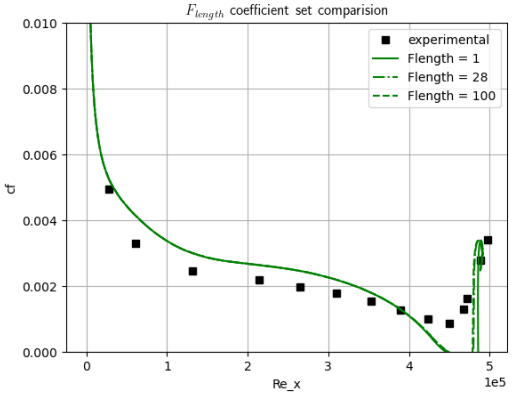

(c) T3C3 c_f

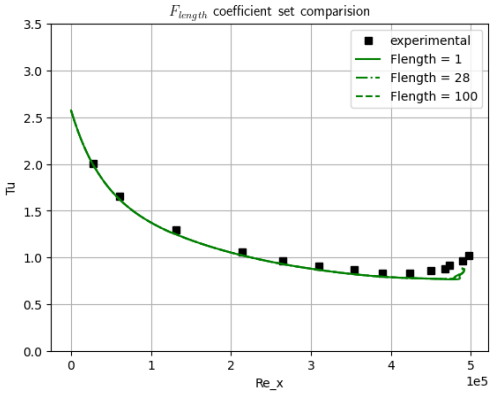

(d) T3C3 Tu

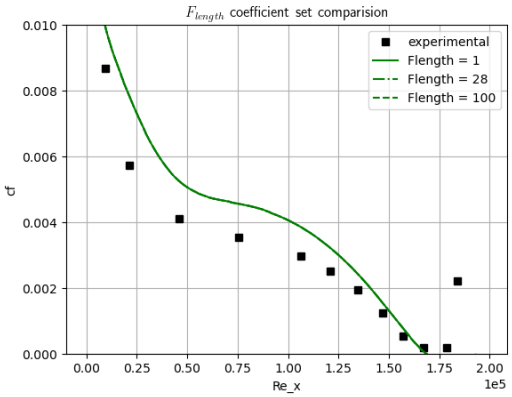

(e) T3C4 c_f

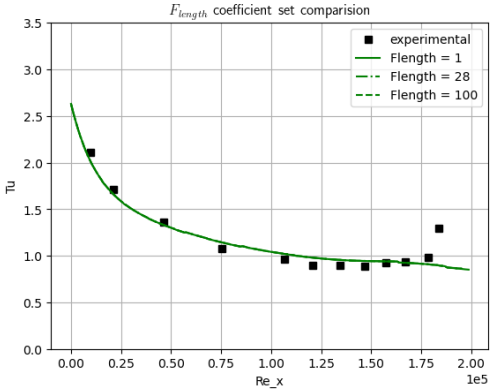

(f) T3C4 Tu

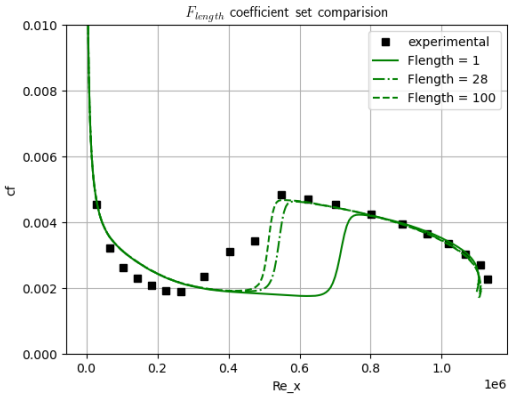

(g) T3C5 c_f

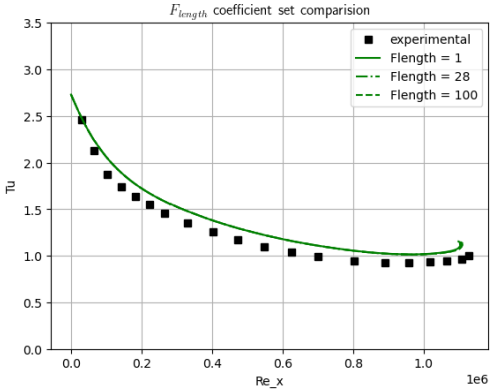

(h) T3C5 Tu

Figure 3.10: Results from coefficient calibration on adverse pressure gradient cases showed on transition curve

the figure 3.12. Turbulence intensity graphs were not included as they remained the same. In the zero pressure gradient case, their transition curves remained similar to the previous optimisation. Worst results showed the case T3A- with the late transition. One problem with COBYLA results was the separation which occurred in cases T3C2 and T3C3. In T3C2, SHGO found a better transition to the turbulent boundary layer and does not dive with c_f below zero. However, it still stays in the laminar region much longer and therefore diverges from experiments. Case T3C3 optimised with SHGO also does not have a region of separation but exhibits a similar quick fall and rise of C_f not present in the experimental data. Recovery in T3C4 was not successful, even with tuned coefficients.

F3 function

Even though we are satisfied with the results obtained by the calibration, we decided to try a further improvement of the $\gamma - EARSM$ turbulence model, so we focused on the F_3 function from $\gamma - SST$ model. Concretely, this function secures that in the the laminar region, $k-\omega$ formulation is ensured. The formulation of the function is as follows

$$f_{mix} = \max(f_{mix}^{orig}, F_3) \qquad F_3 = e^{-\left(\frac{R_y}{120}\right)^8} \qquad R_y = \frac{\rho y \sqrt{k}}{\mu} \tag{3.8}$$

Before the implementation of F_3 function, we examined the behaviour of f_{mix} function and the cross-diffusion term in the ω-equation. In the figure 3.11 we see, that without the F3 function,

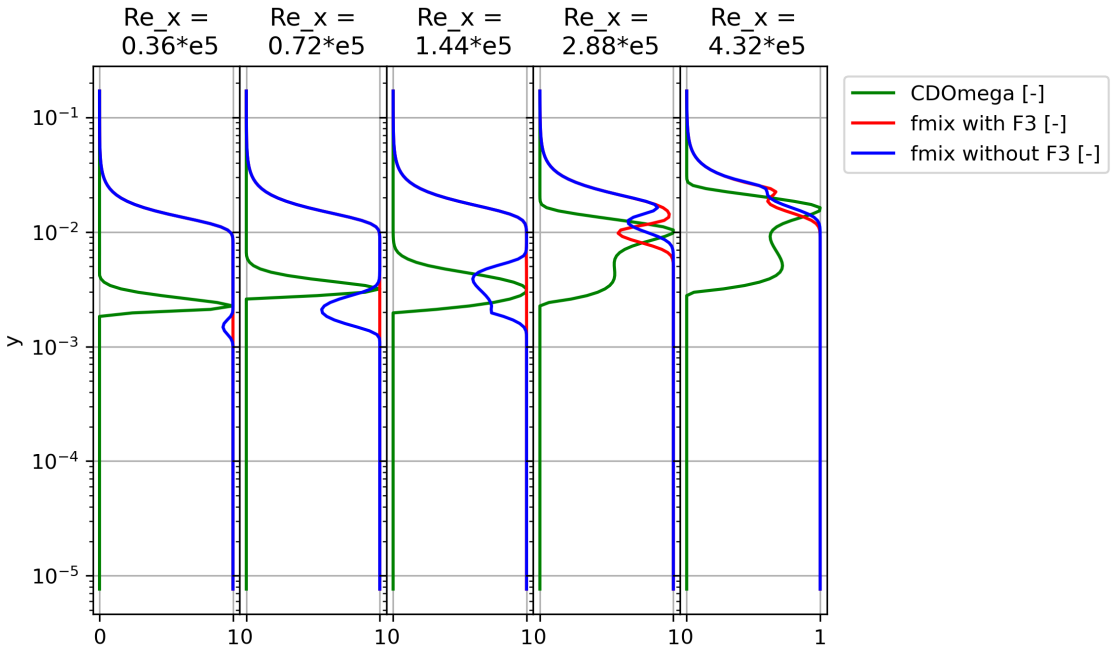

Figure 3.11: Comparison of f_{mix} functions with and without F3 limiter and cross diffusion therm

f_{mix} switches coefficients to the of the $k-\epsilon$ model. This is the region where the transition from laminar to turbulent occurs. As Langtry stated, this is not a desired behavior as we want to have $k-\omega$ in the laminar and transition region [2]. We can also see that the cross-diffusion is active in

this region as well. The cross-diffusion term $\left(\frac{\partial k}{\partial x_j}\frac{\partial \omega}{\partial x_j}\right)$ in the 3.11 is computed with f_{mix} limited by F3. Therefore, in this region we have a formulation of $k-\omega$ with the cross-diffusion term ,however, with coefficients as calibrated by Hellsten. This differs from Langtry[2] implementation. They used a formulation without cross-diffusion term in the boundary region. Based on [2] we have implemented the F3 function and did another SHGO optimization with the same settings and for $F_{length} = 28$. The results are then compared with the previous optimization in the figure 3.12.

3.2 Results

3.2.1 Calibration results

The level of fit is, as expected, certainly a trade-off to fit all test cases. The best fit of the newly proposed model occurs when the transition happens for both average levels of turbulence intensity and velocity inlet. Such cases are T3A and T3C5. We can, however, see that in all cases, the transition is steeper than with $\gamma - SST$.

Cases with high transitional Reynolds number Re_c such as T3C2, T3C3 & T3C4 do not respond swiftly enough to mimic the experiment. In the case of the model without F3 function, it undoubtedly vivacious is that cases T3C2 and T3C3 were able to recover without creating separation. However, in the case of T3C4, there is a significant separation in our numerical results, and the flow was not able to reattach itself before the plate end.

In the case with the F3 function, the results are comparably worse than both optimisation results without the F3 function. Especially in the cases with a pressure gradient, the separation is undoubtedly not in adherence with the experiment. That being said, we do think that the incorporation of the F3 function is the correct step. It is possible, however, that the shorter optimisation time has to be extended.

3.2.2 Further notes

Note that in the T3C3 case's end, there is a visible curl backwards of C_f. The formulation of Re_x causes this curl. In the simplest case, $Re_x = Re_x(u, x)$, where the velocity is from free-stream flow above the boundary layer. As the plate ends with a diverging section, the speed is dropping. This negative velocity gradient causes the seeming effect that the flow does not reach the plate end. To see the transition more clearly, see 3.13. This figure shows that the turbulence model catches the transition correctly. In the case of T3A- $\gamma - EARSM$ reacts too late and to a much higher skin friction coefficient, but this is a slightly an edge case, as the inlet velocity is four times higher than in T3A. Furthermore, the transition occurs at the flat plate end, and thus even though the transition happened later than we want, we do not have enough data to state the performance of our calibration in this case. Therefore, an inevitable error is expected. The same is true for T3B, where both velocity and turbulence intensity are above average. This error is probably due to the much higher turbulence intensity on the inlet, but the curve response is not severe enough to match

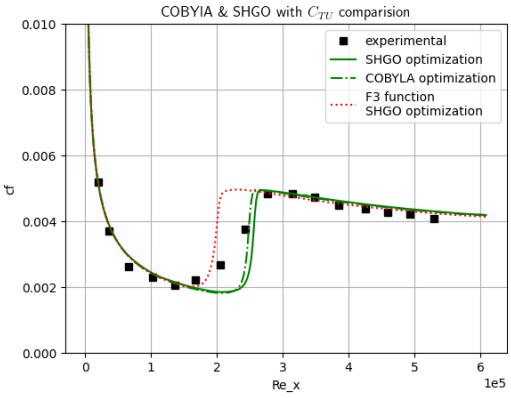

(a) T3A c_f

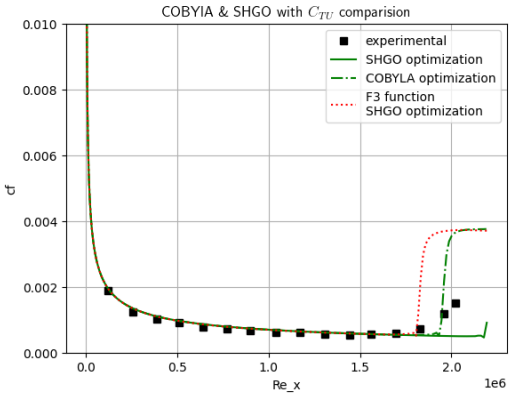

(b) T3A- c_f

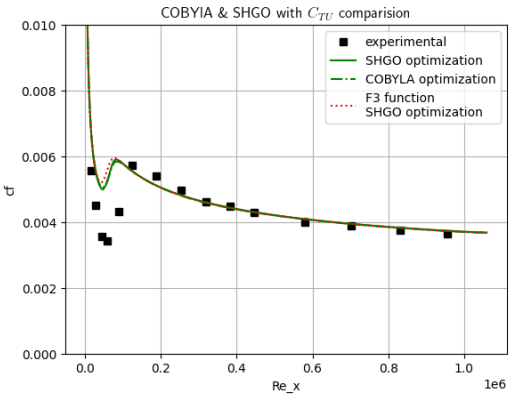

(c) T3B c_f

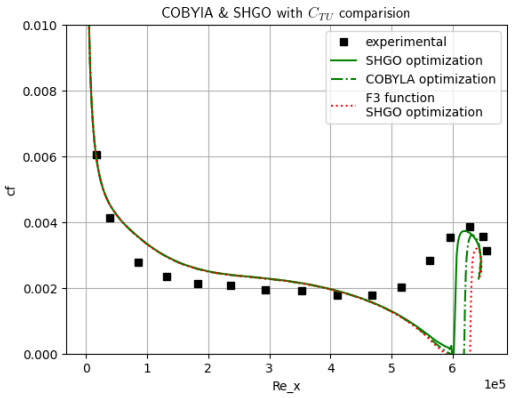

(d) T3C2 c_f

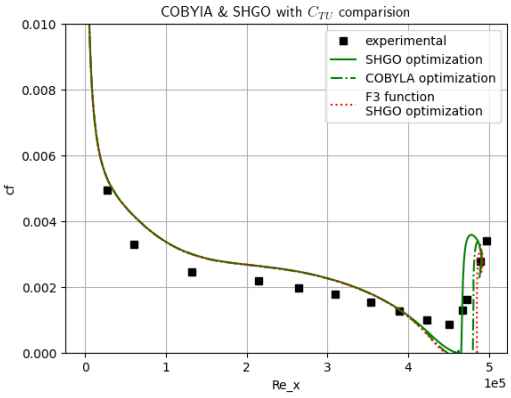

(e) T3C3 c_f

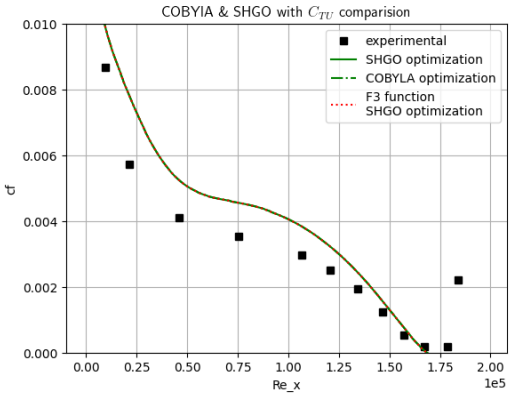

(f) T3C4 c_f

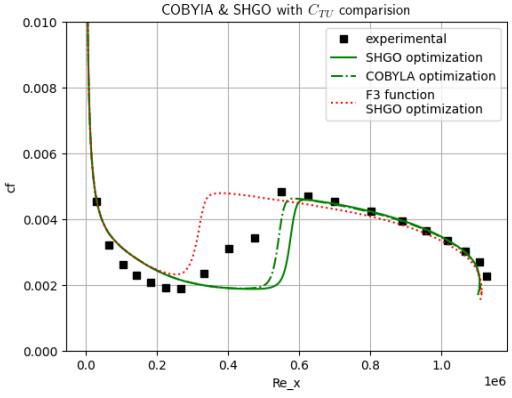

(g) T3C5 c_f

Figure 3.12: SHGO optimization results on cases transition curves

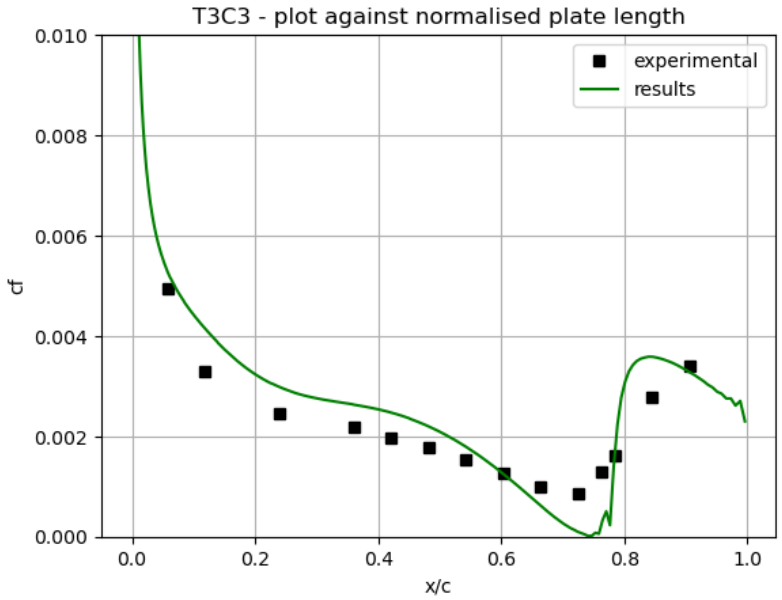

Figure 3.13

the experimental data. Turbulence intensity decays in almost all cases follow the experimental data closely.

Another compromise rests in C_{PG2} where we had to use a significantly higher value than the original. These values result in triggering a transition in the zero pressure gradient case. In theory, this should not happen as there is no pressure gradient. However, this phenomenon stems from the definition of $\lambda_{\Theta L}$, which calculates the pressure gradient in the boundary layer using the term dV/dy. This velocity gradient produces $\lambda_{\Theta L}$ in the zero pressure gradient case as well. The area of non-zero $\lambda_{\Theta L}$ in figure 3.14 is a wedge-shaped area near the flat plate. It originates in the middle of the plate and develops along with the flat plate towards the end.

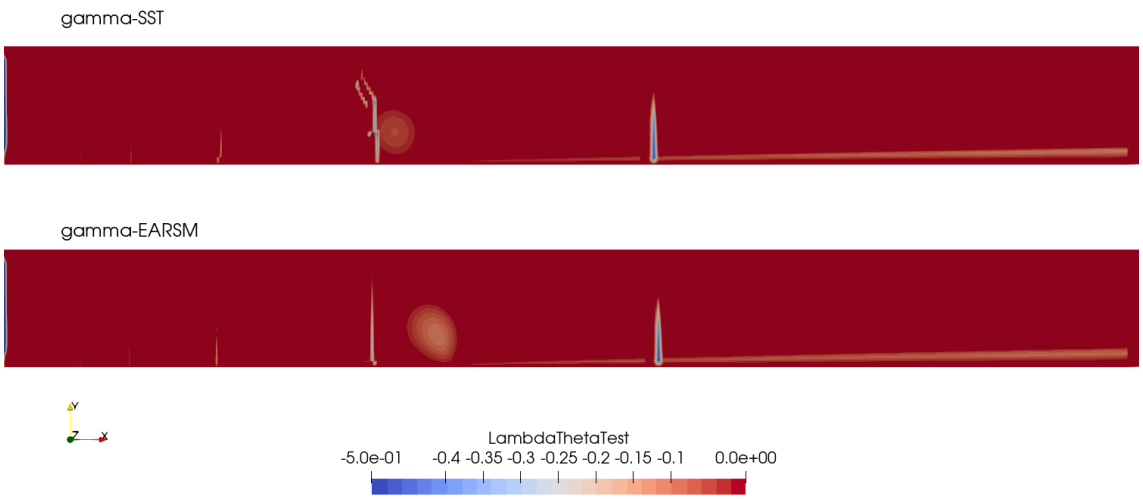

Figure 3.14: $\lambda_{\theta L}$ for both $\gamma - SST$ and $\gamma - EARSM$

3.2.3 Summary of the model

Based on both the results from calibration and the results from validation simulations, we propose a new turbulence model together with a set of coefficients for the intermittency equation. The formulation of our turbulence model is as follows

$$\begin{aligned}
\frac{\mathrm{D}k}{\mathrm{D}t} &= \gamma\mu_t S\Omega + P_k^{lim} - max(\gamma, 0.1) * \beta^* k\omega + \frac{\partial}{\partial x_j}\left[(\nu + \sigma_k\nu_T)\frac{\partial k}{\partial x_j}\right] \\
\frac{\mathrm{D}\omega}{\mathrm{D}t} &= \gamma_{earsm}\frac{\omega}{k}P - \beta\omega^2 + \frac{\partial}{\partial x_j}\left[(\nu + \sigma_\omega\nu_T)\frac{\partial \omega}{\partial x_j}\right] + \frac{\sigma_d}{\omega}\max\left(\frac{\partial k}{\partial x_j}\frac{\partial \omega}{\partial x_j}; 0\right), \\
\frac{\mathrm{D}\gamma}{\mathrm{D}t} &= P_\gamma - E_\gamma + \frac{\partial}{\partial x_j}\left[\left(\mu + \frac{\mu_t}{\sigma_\gamma}\right)\frac{\partial \gamma}{\partial x_j}\right]
\end{aligned} \tag{3.9}$$

where the coefficients in the mixing function f_{mix} were taken over in the form For the equation of

	γ_{earsm}	β	σ_k	σ_ω	σ_d
Set 1	0.518	0.0747	1.1	0.53	1.0
Set 2	0.44	0.0828	1.1	1.0	0.4

Table 3.4: EARSM coefficients for the standard formulation of $k-\omega$ [3]

intermittency, these are the standard coefficients, which we have not altered, see:

$$c_{e2} = 50; \quad c_{a2} = 0.06; \quad \sigma_\gamma = 1.0 \tag{3.10}$$

Below are written out the coefficients of the production term, which are the result of our calibration.

with F3 function

Concretely, these coefficients are tuned using the formulation with the F3 function. The coefficients below have the most significant effect on the zero pressure gradient. However, they retain the original function and thus are tunable by the user.

$$F_{length} = 28.0; \quad C_{TU1} = 110; \quad C_{TU2} = 2000.0; \quad C_{TU3} = 0.85 \tag{3.11}$$

These coefficients are specifically from F_{PG} function and are active in regions with pressure gradient. They are tunable by the user as well, however, because of their interconnected nature, their tuning requires deeper involvement.

$$\begin{aligned}
&C_{PG1} = 100.0; && C_{PG1lim} = 1.5; \\
&C_{PG2} = -7.34; && C_{PG2lim} = 10.0; \qquad C_{PG3} = 0.0
\end{aligned} \tag{3.12}$$

without F3 function

Furthermore, we are writing out the results of optimization without F3 function as well.

$$F_{length} = 28.0; \quad C_{TU1} = 20.0; \quad C_{TU2} = 1100.0; \quad C_{TU3} = 0.2 \tag{3.13}$$

$$\begin{aligned}
&C_{PG1} = 55.0; && C_{PG1lim} = 1.5; \\
&C_{PG2} = -50.5; && C_{PG2lim} = 5.5; \qquad C_{PG3} = 0.0
\end{aligned} \tag{3.14}$$

4. Aplication cases

For the applications below, we chose to mainly calculate the results with f_{mix} limited by the F3 function. However, specific results without the F3 function are added to show the difference in the cases outside of the calibration cases.

4.0.1 Turbine cascade

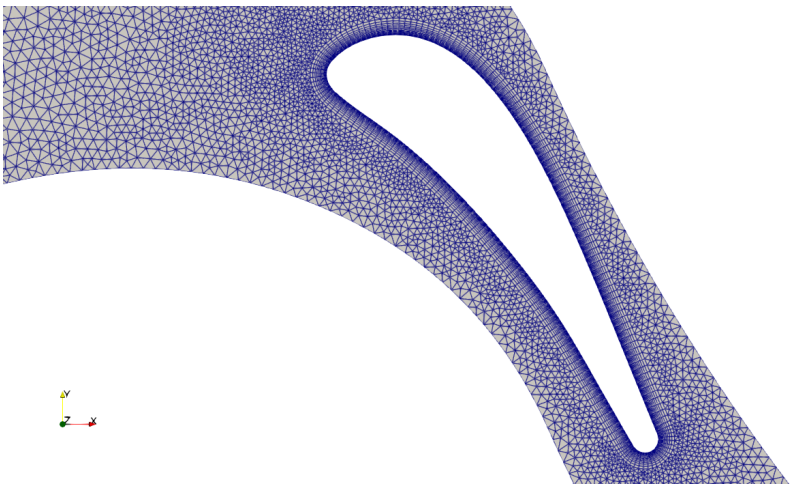

Figure 4.1: Turbine blade mesh

This case is based upon an experiment done in Genova University, Aerodynamics and Turbomachinery Laboratory. Specifically, the experiment consists of a three-blade linear cascade installed in an open-loop type wind tunnel. The blade design is to embody the typical coolable high-pressure gas turbine nozzle blades. The blade geometry is two-dimensional and was designed by Von Karman Institute for Fluid Dynamics. Only the middle blade in the cascade was instrumented. The whole test section is characterized by chord length $c = 300mm$ pitch-to-chord ratio $g/c = 0.7$, blade aspect ratio $h/c = 1$ and gauging angle = 19.2 deg, see further info at [7]. The simulation is based on a single blade where the profile is visible in picture 4.1. The unstructured 2D mesh used in this simulation was provided by doc. Jiří Furst from the Department of Technical Mathematics, faculty of mechanical engineering, CTU in Prague, and has 18096 cells. The domains consist of velocity inlet, pressure outlet, and periodic boundaries. We calculated the flow field around a single airfoil with the assumption of periodic boundary conditions. In this test case, we compare our numerical results with $\gamma - EARSM$ to $\gamma - SST$ and experimental data. We performed all calculations with Reynolds number equal $5.9{\cdot}10^5$. The maximum value of $y^+ = 0.12$. The simulation was run both as incompressible and compressible with *simpleFoam* and *rhoSimpleFoam* solvers respectively. Inlet conditions respect the test conditions from the experiment, see table 4.1. Looking at the skin friction coefficient comparison, the properties observed during calibration are visible here, namely, the sharper rise from the laminar to the turbulent boundary layer. There is also a visible aft shift

Inlet Condition	Value
T_{t1}	$293K$
Tu	1%
M_{1is}	0.086
Re	$5.9 \cdot 10^6$

Table 4.1: Inlet boundary conditions as used in numerical simulation

of the transition curve, but the skin friction coefficient in the turbulent boundary layer is closer than $\gamma - SST$. The total wall shear stress was calculated between $s/s_{max} = \langle 0.17, 0.91 \rangle$ to exclude oscillations towards the trailing edge. In the table 4.2 $\gamma - EARSM$, we see that it overestimates the experimental value, but still, the values are slightly closer to the experimental value. Results from compressible and incompressible assumptions are in agreement, which serves as further proof for relaying on an incompressible formulation. It should be noted that this comparison is made solely based on skin friction coefficient data. We numerically integrated both experimental and CFD data as we did in an error function for minimization. The velocity was calculated using the

Turbulence model	total wall shear stress
Experiment	1.68e-3
$\gamma - EARSM$ & F3 (simpleFoam)	1.69e-3
$\gamma - SST$ (simpleFoam)	1.60e-3
$\gamma - EARSM$ (simpleFoam)	1.72e-3

Table 4.2: Inlet boundary conditions as used in numerical simulation

isentropic relation, which is based on the assumption of ideal flow. This assumption is visible around x/c=0.6, a slight dip in the isentropic velocity compared to the experimental values. This corresponds well with our skin friction plot, where at this coordinate, we can see the transition from laminar to turbulent occurring. In the figure 4.2 is comparison of boundary layer velocities with experimental and $\gamma - SST$ results. The difference between the turbulence models is negligible, yet there is a slight offset between numerical and experimental data. However, the trend of the curves is similar and the difference between laminar and turbulent profiles is visible, specifically between $s/s_{max} = 0.52$ and $s/s_{max} = 0.62$. The clock time required for $\gamma - EARSM$ was 8.5% higher compared to $\gamma - SST$

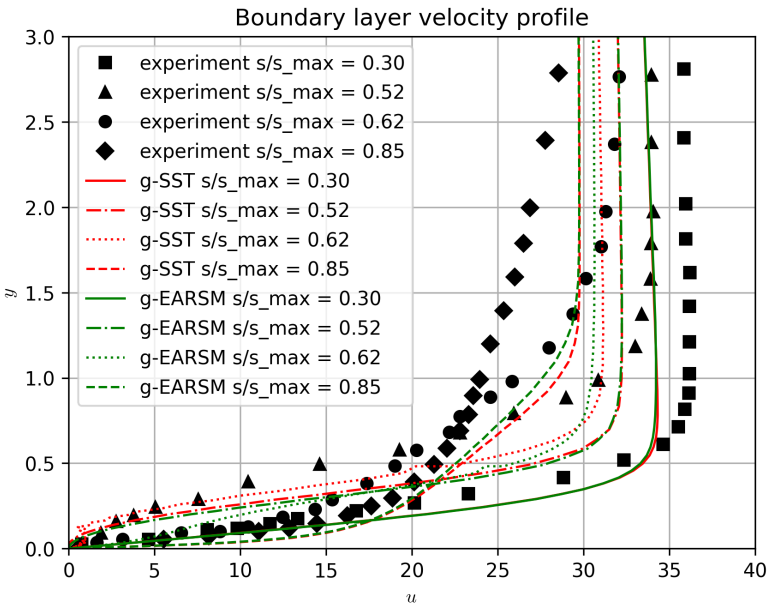

Figure 4.2: Boundary layer velocity profile

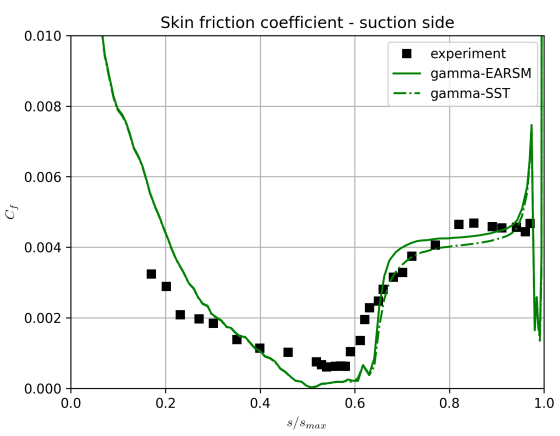

(a) c_f for both turbulence models

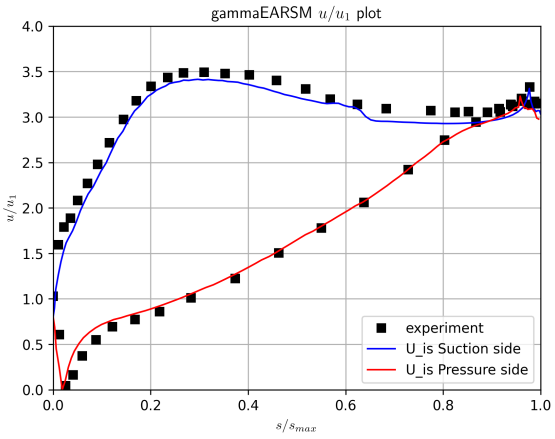

(b) c/c_1 for $\gamma - EARSM$ calculated using simpleFoam

4.0.2 NLF airfoil

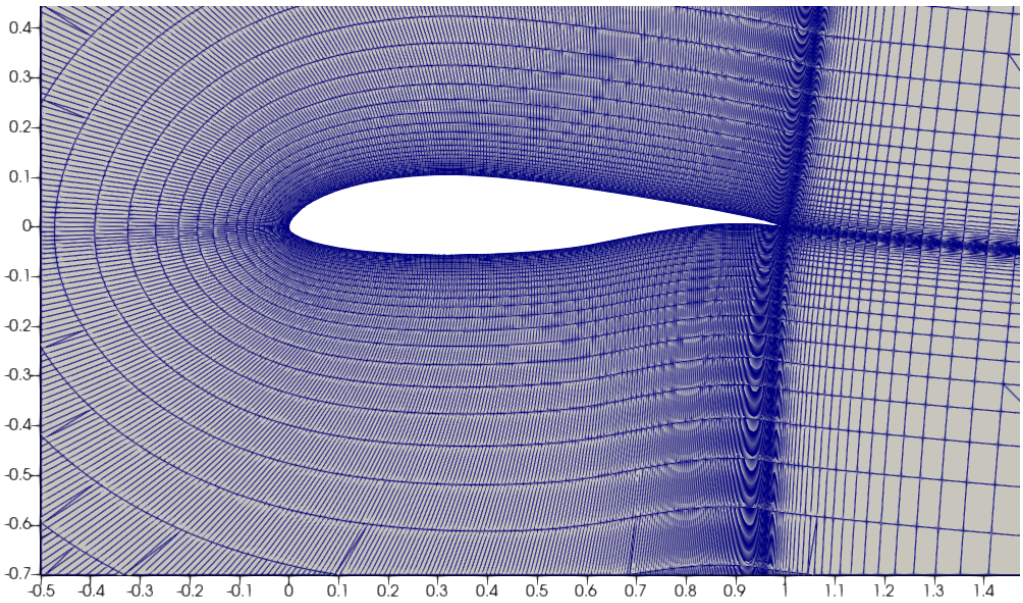

Figure 4.4: NLF-0416 airfoil mesh near view [10]

The simulation is based upon NASA research for natural-laminar-flow airfoil for general aviation applications. The main objective of this design was to create an airfoil that retains up to 30% of the boundary layer in the laminar state and thus achieves low profile drag. The measurement was done in Langley low-turbulence Pressure Tunnel (LTPT). The wind tunnel is of single-return type with a closed throat. The measurements were done for a wide range of flow regimes with variable Reynolds number, Mach number, and surface roughness. For our study, we have chosen a regime with $Re = 4 \cdot 10^6$ and at free-stream $Ma = 0.1$. We have studied the airfoil as two-dimensional with the assumption of compressibility as we expected the local Ma to exceed 0.3. The solver used was therefore *rhoSimpleFoam* as we were looking for a steady-state solution. Since we are using a simplified two-dimensional domain, we were only examining the performance of the airfoil at angles of attack in the range $\langle -4°, 8° \rangle$ with increments of 2°. Examining the airfoil around the maximum lift is hard as we are expecting separation and loss of lift. However, phenomena such as separation are spatial, and thus, our results would reflect the experimental results poorly. The

Inlet Condition	Value
M_{inlet}	0.1
Tu	0.15%
T_{ref}	$540R$
Re	$4 \cdot 10^6$

Table 4.3: Boundary conditions as used in numerical simulation

maximum value of $y^+ = 0.59$. The figure compares the lift coefficient between $\gamma - EARSM$ and $\gamma - SST$, where the fit of both turbulence models is practically the same. From the comparison

of c_p, we can see that $\gamma - EARSM$ has a slightly better fit. Both models overpredict the pressure coefficient in the peaks at the leading edge of the airfoil. The slope of the curves aft of the pressure coefficient peak is correct. On the lower surface, we can see that both turbulence models transition from laminar to turbulent at $x/c \approx 0.65$, which agrees with the experimental data. At $Re = 4 \cdot 10^6$, the upper surface boundary layer should be, for the most part, turbulent. We can see that $\gamma - SST$ holds laminar boundary layer up to $x/c \approx 0.18$ and $\gamma - EARSM$ transitions at around the same level. Without the F3 function, the transition is around$x/c \approx 0.05$. Based on the paper, the transition location should be around $x/c \approx 0.12$ for our lift coefficient value $c_l = 1.31$.

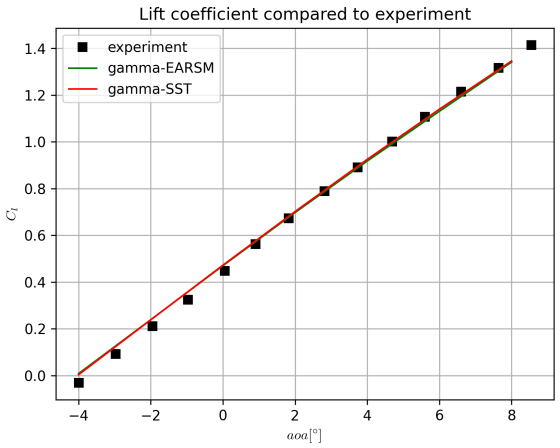

(a) c_l comparison for both turbulence models

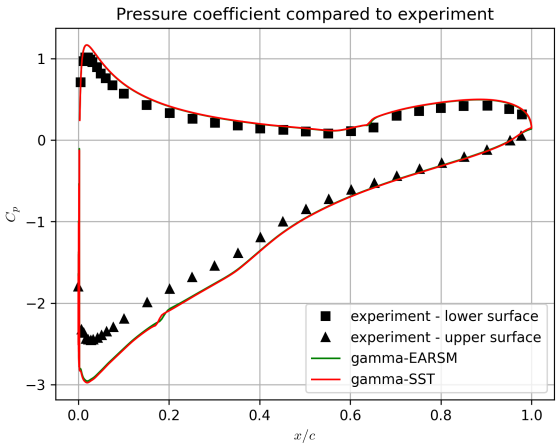

(b) c_p comparison for both turbulence models at anlge of attack 8°

5. Conclusion

A new transitional turbulence model based on explicit algebraic Reynolds stress has been developed and tested. The model is formulated with the EARSM model as its primary model for solving k and ω, developed by Hellsten. Further, it is coupled with a transitional model $\gamma - SST$ developed by Menter; Smirnov; Liu; Avancha. From the $\gamma - SST$ we took the partial differential equation for intermittency. The advantage is that its part of the Local Correlation-based Transition Modeling family of models. Thus all correlations for the transition are calculated locally, contrary to $\gamma - Re_\theta$. In addition, both $\gamma - SST$ and EARSM are Galilean invariant, which means that they are dependent only on a local frame of reference, which is suitable for applications, for instance, in turbo-machinery.

Concretely, the EARSM model improves the Boussinesq approximation by replacing it with a constitutive model containing effective eddy viscosity and extra anisotropy. Thus, it can model some of the flow properties which stem from turbulence anisotropy, such as the effects of streamline curvature.

The equation for intermittency was added to allow us to broaden the range of applications of the EARSM model to applications where boundary layer transition and separation play a role.

Calibration of the $\gamma - EARSM$ model was done by calculation of incompressible two-dimensional flat plate flow and compared with ERCOFTAC flat plate experimental measurements. This experiment provides data on boundary layer development along a flat plate under diverse flow conditions. Flows under both zero-pressure gradient and adverse pressure gradient were used for the calibration to broaden the capabilities of the newly calibrated model. In this thesis, we only calibrated the production terms in the intermittency equation, yet we achieved a good fit to the experimental data. The calibration was done with the help of optimisation algorithms, concretely SHGO & COBYLA algorithms were used, where the final optimisation was done using SHGO. We chose the total wall shear stress on the flat plate as a performance metric and minimised the difference between experimental and numerical data. We provided two formulations, with and without the modified blending function. The modified formulation was taken from Menter; Smirnov; Liu; Avancha to secure $k - \omega$ model in the laminar boundary layer. The computational effort did not rise substantially over the $\gamma - SST$.

For validation, we chose an internal and external flow around an airfoil. Concretely, for the external aerodynamics, we chose NFL-0416 airfoil, and for the internal, we opted for a linear blade cascade with blade design from VKI. Obtained results showed slightly improved performance in contrast to $\gamma - SST$. Notably, the formulation with blending function performed on par even though the performance on calibration cases was weak. Areas of improvement are the extension of optimisation time or improve the optimisation process to manage more calculations. However, further validation would be required to truly see the benefits of combining the transitional turbu-

lence model and algebraic Reynolds stress.

Further development of better coefficients will be done in the future, as well as tests of turning off the cross-diffusion term with the modified blending function.

Bibliography

1. SAVILL, A M. Chapter 6: ONE-POINT CLOSURES APPLIED TO TRANSITION. *One-Point Closures Applied to Transition*. 1996, vol. 2, pp. 233–268.
2. LANGTRY, R. B. A Correlation-Based Transition Model Using Local Variables for Unstructured Parallelized CFD codes. *Journal of Turbomachinery*. 2006, vol. 128, no. 3, p. 413. ISBN 0791841693. ISSN 0889504X. Available from DOI: 10.1115/1.2184352.
3. HELLSTEN, Antti. *New two-equations turbulence model for aerodynimic flows*. 2004. ISBN 951-22-6934-1. Available also from: http://lib.tkk.fi/Diss/2004/isbn9512269341/.
4. MENTER, Florian R.; SMIRNOV, Pavel E.; LIU, Tao; AVANCHA, Ravikanth. A One-Equation Local Correlation-Based Transition Model. *Flow, Turbulence and Combustion*. 2015, vol. 95, no. 4, pp. 583–619. ISSN 1386-6184. Available from DOI: 10.1007/s10494-015-9622-4.
5. POPE, Stephen B. *Turbulent Flows*. 2000. ISBN 9780511840531. ISSN 0957-0233. Available from DOI: 10.1088/0957-0233/12/11/705.
6. WALLIN, Stefan; JOHANSSON, Arne V. Modelling streamline curvature effects in explicit algebraic Reynolds stress turbulence models. *International Journal of Heat and Fluid Flow*. 2002, vol. 23, no. 5, pp. 721–730. ISSN 0142727X. Available from DOI: 10.1016/S0142-727X(02)00168-6.
7. SMITH, A. High-lift aerodynamics /37th Wright Brothers Lecture/. 1974, vol. 12, no. 6. Available from DOI: 10.2514/6.1974-939.
8. MENTER, F. R. Two-equation eddy-viscosity turbulence models for engineering applications. *AIAA Journal*. 1994, vol. 32, no. 8, pp. 1598–1605. ISSN 00011452. Available from DOI: 10.2514/3.12149.
9. SULUKSNA, Keerati; DECHAUMPHAI, Pramote; JUNTASARO, Ekachai. Correlations for modeling transitional boundary layers under influences of freestream turbulence and pressure gradient. *International Journal of Heat and Fluid Flow*. 2009, vol. 30, no. 1, pp. 66–75. ISSN 0142727X. Available from DOI: 10.1016/j.ijheatfluidflow.2008.09.004.
10. SOMERS, Dan M. DESIGN AND EXPERIMENTAL RESULTS FOR A FLAPPED NATURAL-LAMINAR-FLOW AIRFOIL FOR GENERAL AVIATION APPLICATIONS. *NASA Technical Paper*. 1981, no. June 1981. ISSN 01488341.
12. POWELL, M J D. *A view of algorithms for optimization without derivatives 1*. 2007. Tech. rep.
13. KUNDE, Vliegtuigbouw. van KARMAN INSTITUTE. 1990, no. September.

14. ROACHE, Patrick J. *Computing in Science Engineering*. Verification and Validation in Computational Science and Engineering. 1998. ISBN 0913478083. Available also from: `http://www.hermosa-pub.com/hermosahttp://scholar.google.com/scholar?hl=en{\&}btnG=Search{\&}q=intitle:Verification+and+validation+in+computational+science+and+engineering{\#}0`.

15. ABU-GHANNAMT, B J; SHAWSS, R. *NATURAL TRANSITION O F BOUNDARY LAYERS-THE EFFECTS OF TURBULENCE, PRESSURE GRADIENT, AND FLOW HISTORY*. Tech. rep.

16. STEED, Robin. *High Lift CFD Simulations with an SST-Based Predictive Laminar to Turbulent Transition Model*. 2010. Tech. rep.

17. WALLIN, Stefan. Engineering turbulence modelling for CFD with a focus on explicit algebraic Reynolds stress models by. *Ph D thesis Royal Institute of Technology Stockholm*. 2000, no. February, p. 244. Available also from: `http://www.mech.kth.se/thesis/2000/phd/phd{\_}2000{\_}stefan{\_}wallin.pdf`.

18. POPE, S B. *A more general effective-viscosity hypothesis*. 1975. Tech. rep., 2.

19. SAVILL, A. M. Evaluating turbulence model predictions of transition. *Applied Scientific Research*. 1993, vol. 51, no. 1, pp. 555–562. ISSN 1573-1987. Available from DOI: `10.1007/BF01082590`.

20. VIRTANEN, Pauli; GOMMERS, Ralf; OLIPHANT, Travis E.; HABERLAND, Matt; REDDY, Tyler; COURNAPEAU, David; BUROVSKI, Evgeni; PETERSON, Pearu; WECKESSER, Warren; BRIGHT, Jonathan; VAN DER WALT, Stéfan J.; BRETT, Matthew; WILSON, Joshua; MILLMAN, K. Jarrod; MAYOROV, Nikolay; NELSON, Andrew R. J.; JONES, Eric; KERN, Robert; LARSON, Eric; CAREY, C J; POLAT, İlhan; FENG, Yu; MOORE, Eric W.; VANDERPLAS, Jake; LAXALDE, Denis; PERKTOLD, Josef; CIMRMAN, Robert; HENRIKSEN, Ian; QUINTERO, E. A.; HARRIS, Charles R.; ARCHIBALD, Anne M.; RIBEIRO, Antônio H.; PEDREGOSA, Fabian; VAN MULBREGT, Paul; SCIPY 1.0 CONTRIBUTORS. SciPy 1.0: Fundamental Algorithms for Scientific Computing in Python. *Nature Methods*. 2020, vol. 17, pp. 261–272. Available from DOI: `10.1038/s41592-019-0686-2`.

21. POWELL, M. J. D. A Direct Search Optimization Method That Models the Objective and Constraint Functions by Linear Interpolation. In: *Advances in Optimization and Numerical Analysis*. Springer Netherlands, 1994, pp. 51–67. Available from DOI: `10.1007/978-94-015-8330-5_4`.

22. PIRONNEAU, Olivier. *Numerical simulation of unsteady flows and transition to turbulence : proceedings of the ERCOFTAC Workshop held at EPFL, 26-28 March 1990, Lausanne, Switzerland*. Cambridge England New York, NY, USA: Cambridge University Press, 1992. ISBN 978-0521416184.

23. *ERCOFTAC Flat Plate Transitional Boundary Layers*. 2020. Available also from: http://cfd.mace.manchester.ac.uk/ercoftac/doku.php?id=cases%3Acase020.

24. J. PŘÍHODA, P. Louda. *Matematické modelování turbulentního proudění*. [N.d.].

25. CHIEN, Kuei-Yuan. Predictions of Channel and Boundary-Layer Flows with a Low-Reynolds-Number Turbulence Model. *AIAA Journal*. 1982, vol. 20, no. 1, pp. 33–38. Available from DOI: 10.2514/3.51043.

26. WILCOX, D. Formulation of the k-w Turbulence Model Revisited. *AIAA Journal*. 2008, vol. 46, pp. 2823–2838.